SYNTHESIS OF FLOWER-SHAPED COPPER FERRITE WITH COPPER AND IRON EXTRACTED FROM THE DIFFERENT ACID TREATMENTS OF CHALCOPYRITE FOR SUPERCAPACITOR ELECTRODE APPLICATION

2022
MASTER THESIS
METALLURGY AND MATERIALS ENGINEERING

El Moctar MBEBOU

Thesis Advisor
Assist. Prof. Dr. Safa POLAT

SYNTHESIS OF FLOWER-SHAPED COPPER FERRITE WITH COPPER AND IRON EXTRACTED FROM THE DIFFERENT ACID TREATMENTS OF CHALCOPYRITE FOR SUPERCAPACITOR ELECTRODE APPLICATION

T.C.
Karabuk University
Institute of Graduate Programs
Department of Metallurgy and Materials Engineering
Prepared as
Master Thesis

El Moctar MBEBOU

Thesis Advisor
Assist. Prof. Dr. Safa POLAT

KARABUK
December 2022

I certify that in my opinion the thesis submitted by El Moctar MBEBOU titled "SYNTHESIS OF FLOWER-SHAPED COPPER FERRITE WITH COPPER AND IRON EXTRACTED FROM THE DIFFERENT ACID TREATMENTS OF CHALCOPYRITE FOR SUPERCAPACITOR ELECTRODE APPLICATION " is fully adequate in scope and in quality as a thesis for the degree of Master of Science.

Assist. Prof. Dr. Safa POLAT .....
Thesis Advisor, Department of Metallurgical and materials Engineering

This thesis is accepted by the examining committee with a unanimous vote in the Department of Computer Engineering as a Master of Science thesis.
December 26, 2022

Examining Committee Members (Institutions)	Signature
Chairman : Assoc. Prof. Dr. Muhammet Emre TURAN (KBU)	.....
Member : Assist. Prof. Dr. Safa POLAT (KBU)	.....
Member : Assoc. Prof. Dr. Adem YAR (BU)	Online

The degree of Master of Science by the thesis submitted is approved by the Administrative Board of the Institute of Graduate Programs, Karabuk University.

Assoc. Dr. MÜSLÜM KUZU .....
Director of the Institute of Graduate Programs

"I declare that all the information within this thesis has been gathered and presented in accordance with academic regulations and ethical principles and I have according to the requirements of these regulations and principles cited all those which do not originate in this work as well."

El Moctar MBEBOU

ABSTRACT

M. Sc. Thesis

SYNTHESIS OF FLOWER-SHAPED COPPER FERRITE WITH COPPER AND IRON EXTRACTED FROM THE DIFFERENT ACID TREATMENTS OF CHALCOPYRITE FOR SUPERCAPACITOR ELECTRODE APPLICATION

Karabuk University

Institute of Graduate Programs

Department of Metallurgy and Materials Engineering

El Moctar MBEBOU

Thesis Advisor:

Assist. Prof. Dr. Safa POLAT

December 2022, 72 pages

Supercapacitors are one of the important energy storage systems that emerged as an alternative to lithium-ion batteries. The development of their electrodes is one of the important scientific study areas that has gained momentum in recent years. In this context, many syntheses have been carried out so far by considering the charge storage mechanisms of the electrodes. These are based on the principle of physical and chemical attachment of ions on the electrode surfaces. The physical attachment of the ions is related to the surface area of the electrode, and the chemical attachment is related to the oxidation/reduction mechanisms occurring on the surface. Two different components have generally been used in the studies to perform these operations. However, a single-component component that can perform both tasks is designed in this thesis. For this purpose, nano-sized metal oxide synthesis was carried out on the

nickel foam current collector electrode surface from a natural mineral. Chalcopyrite containing copper and iron elements, which can give an easy redox reaction, was chosen as a mineral. First, chalcopyrite mineral was treated with 10-20-30-40 ppm concentrations of HCl, H_2SO_4, and HNO_3 acids to extract copper and iron. Atomic absorption spectroscopy (AAS) was used to determine copper and iron concentrations in each solution. Afterward, the obtained results were compared with acid-free extraction, and optimization was achieved. After that, the highest copper and iron extraction was determined as 492 ppm with 446 ppm of HNO_3 acid. The second step aims to produce copper ferrite-based electrodes with this solution containing the highest concentration of copper and iron. This synthesis process was carried out on the surface of the nickel foam used in the productions. After that, FTIR, XRD, TEM, and SEM techniques were used to describe the generated electrodes in terms of the chemical bond structures, crystal planes, and microstructures, respectively. Then, the electrochemical performance of the produced electrode was determined using cyclic voltammetry (CV) and galvanostatic charge-discharge measurements (GCD) with a three-electrode setup. The obtained characterization results showed that the flower-shaped $CuFe_2O_4$ was successfully synthesized on the nickel foam surface despite some impurities. Electrochemical results showed that the electrode has a battery-type charging mechanism, and the highest specific capacitance is 525 mF/cm^2 at 2 mA/cm^2 current density. In addition, this electrode's energy and power densities at a current density of 2 mA/cm^2 were calculated as 8.9 mWh/cm2 and 233 mWh/cm^2. As a result, it has been discovered that copper and iron extraction from chalcopyrite can be conducted at higher rates than their counterparts in the literature while using a low-cost component such as nitric acid. Furthermore, it has been established that the solution developed here can create high-performance electrodes for supercapacitors, a key component of energy storage devices. The electrochemical performances of the produced electrodes were seen to be promising for supercapacitors in this context; nonetheless, it was decided that additional research is required to determine whether this is the case.

Key Words: Chalcopyrite, extraction, nanoplate, metal oxide, hydrothermal method, supercapacitor.

Science Code : 91520, 91530

ÖZET

Yüksek Lisans Tezi

SÜPER KAPASİTÖR ELEKTROT UYGULAMASI İÇİN KALKOPİRİTİN FARKLI ASİT İŞLEMLERİNDEN ELDE EDİLEN BAKIR VE DEMİR İLE ÇİÇEK BİÇİMLİ BAKIR FERRİT SENTEZİ

Karabük Üniversitesi
Lisansüstü Eğitim Enstitüsü
Metalurji ve Malzeme Mühendisliği Anabilim Dalı

El Moctar MBEBOU

Tez Danışmanı:
Dr. Öğr. Üyesi Safa POLAT
Eylül 2022, 72 sayfa

Süper kapasitörler, lityum-iyon pillere alternatif olarak ortaya çıkan önemli enerji depolama sistemlerinden biridir. Süperkapasitör elektrotlarının geliştirilmesi ise son yıllarda ivme kazanan önemli bilimsel çalışma alanlarından biridir. Bu bağlamda elektrotların yük depolama mekanizmaları dikkate alınarak bugüne kadar birçok çalışma yapılmıştır. Bunlar, iyonların elektrot yüzeylerine fiziksel ve kimyasal bağlanması prensibine dayanmaktadır. İyonların fiziksel bağlanması elektrotun yüzey alanıyla, kimyasal bağlanması ise yüzeyde meydana gelen yükseltgenme/indirgeme mekanizmalarıyla ilgilidir. Bu işlemleri gerçekleştirmek için literatürdeki yapılan çalışmalarda genellikle iki farklı bileşen kullanılmaktadır. Ancak bu tez çalışmasında her iki görevi de yerine getirebilen tek bir bileşen tasarlanması planlanmıştır. Bu amaçla, doğal bir mineralden akım toplayıcı nikel köpük elektrot yüzeyinde nano boyutlu metal oksit sentezi gerçekleştirilmiştir. Mineral olarak kolay redoks

reaksiyonu verebilen bakır ve demir elementleri içeren kalkopirit seçilmiştir. İlk olarak kalkopirit minerali 10-20-30-40 ppm konsantrasyonlarında HCl, H_2SO_4 ve HNO_3 asitleri ile muamele edilerek bakır ve demir elde edilmiştir. Her çözeltideki bakır ve demir konsantrasyonlarını belirlemek için atomik absorpsiyon spektroskopisi (AAS) kullanılmıştır. Daha sonra elde edilen sonuçlar asitsiz ekstraksiyon ile karşılaştırılarak optimizasyon sağlanmıştır. Ekstraksiyon sonrası en yüksek bakır ve demir konsantrasyonları HNO_3 asit solüsyonunda sırasıyla 446 ppm ve 492 ppm olarak belirlenmiştir. İkinci adımda en yüksek konsantrasyonlu bu solüsyon ile bakır ferrit bazlı elektrot üretimi gerçekleştirilmesi amaçlanmıştır. Bu sentezler nikel köpük yüzeyinde hidrotermal yöntem ile doğrudan gerçekleştirilmiştir. Üretilen elektrotların öncelikle kimyasal bağları, kristal düzlemleri ve mikro yapıları FTIR, XRD, TEM ve SEM analizleri ile karakterize edilmiştir. Daha sonra bu elektrotların elektrokimyasal performansları belirlemek için üç elektrotlu bir sistem kullanılarak çevrimli voltametri (CV) ve galvano statik şarj-deşarj ölçümleri (GCD) uygulanmıştır. Elde edilen karakterizasyon sonuçları, çiçek şeklindeki $CuFe_2O_4$'ün bazı safsızlıklara rağmen nikel köpük yüzeyinde başarılı bir şekilde sentezlendiğini göstermiştir. Elektrokimyasal sonuçlar ise elektrotun pil tipi bir şarj mekanizmasına sahip olduğunu ve en yüksek özgül kapasitansın 2 mA/cm^2 akım yoğunluğunda 525 mF/cm^2 olduğunu göstermiştir. Ayrıca bu elektrotun 2 mA/cm^2 akım yoğunluğundaki enerji ve güç yoğunlukları 8,9 mWh/cm^2 ve 233 mWh/cm^2 olarak hesaplanmıştır. Sonuç olarak nitrik asit gibi son derece düşük maliyetli bir bileşen kullanılarak kalkopiritten bakır ve demir ekstraksiyonunun literatürdeki muadillerinden daha yüksek oranlarda gerçekleştirilebildiği tespit edilmiştir. Ayrıca buradan elde edilen solüsyon ile enerji depolama cihazlarının önemli bir bileşeni olan süper kapasitörler için yüksek performanslı elektrot yapılabileceği sonucuna da varılmıştır. Bu bağlamda elde edilen elektrotların elektrokimyasal performanslarının süper kapasitörler için umut verici olduğuna inanılmış; ancak, durumun böyle olup olmadığını belirlemek için daha fazla araştırma yapılması gerektiği sonucuna varılmıştır.

Anahtar Kelimeler : Kalkopirit, ekstraksiyon, nanoplaka, metal oksit, hidrotermal yöntem, süper kapasitör.

Bilim Kodu **:** 91520, 91530

ACKNOWLEDGMENT

To begin, I would like to express my sincere thanks to the omnipotent Allah for all the blessings and guidance he gave me throughout my investigation.

My gratitude to my adviser, Assist. Prof. Dr. Safa POLAT is profound. To have worked and studied under his leadership was a mesmerizing honor.

With deep gratitude, I acknowledge the following individuals, without whom I would not have been able to carry out my study and get my master's degree.

The Iron and Steel Institute (MARGEM) staff at Karabuk University, whose insights and expertise on the topic guided me through my project. I also want to extend my gratitude to Cheikh Sidi El Moctar Mohamed LEFDHIL, Muwafaq MASHRAH, and Mariem MOHAMED, El Mamy Mariem ABDI, without whom I would not have any content to include in my thesis.

For those who believed in me and helped me get where I am now, I offer my sincerest gratitude and dedicate this work to you, especially my father, Mohamed MBEBOU, my mother, Aichetou ELFOUDHAIL, Mariem MAHMOUDEN, my dear sisters Meymoune MBEBOU, Naha MBEBOU, Bedi MBEBOU, Ibtisam MBEBOU. I want to express my appreciation to my brothers Souleyman MBEBOU, Ahmed MBEBOU, and Abdallahi HAMDEN.

I want to extend my gratitude to my elder brother, Moctar MAHMOUDEN, who has been there for me and invested time and energy into helping me succeed as an outstanding person I respect.

There are no words powerful enough to describe my thanks and love to you, but I sincerely thank you for everything. I recognize all that you have done. I would also like to thank the project numbered KBÜBAP-21-ABP-047 of Karabuk University Scientific Research Projects Unit (KBU-BAP), which provided funding for the analyses.

CONTENTS

Page

Page

LIST OF FIGURES

Page

Page

LIST OF TABLES

Page

SYMBOLS AND ABBREVITIONS INDEX

SYMBOLS

mA	: Milliampere
mg	: Milligram
°C	: Degrees Celsius
K	: Kelvin
s	: Second
Cu	: Copper
mWh/cm^2	: Milliwatts hour per centimeter squared
mW/cm^2	: Milliwatts per centimeter squared
$CuFeS_2$	: Chalcopyrite
Cl	: Chloride
S	: Sulphury

ABBREVITIONS

SEM	: Scanning Electron Microscope
XRD	: X-Ray Diffraction
FTIR	: Fourier Transform Infrared Spectroscopy
AAS	: Atomic absorption spectroscopy
CFO	: Copper ferrite ($CuFe_2O_4$)
CV	: Cyclic voltammetry
GCD	: Galvanostatic charge-discharge

PART 1

INTRODUCTION

The natural world provides people with all they need throughout their whole lives. Utilization of natural resources is required for the development of practically all of the instruments and apparatus that are necessary for effective living. Natural resources may be found in every part of our life, such as the earth, river, wildlife, woods, sunshine, hydrocarbons, raw mineral materials, and even the air that we breathe. Some examples of natural resources include: If we feel the need to categorize these resources according to where they came from, we may separate them into biotic and abiotic categories [1]. Biotic resources are made up of organic materials and lifeforms. Additional natural resources with an organic origin include plants, animals, and fossil fuels including coal, oil, and natural gas. Natural resources with an inorganic (non-living) origin are known as abiotic resources and include things like air, water, sunshine, minerals, and metals [2].

Materials and alloys are among the natural resources that are crucial for a country's socioeconomic growth. Additionally, it satisfies the fundamental raw material requirements of the energy sector and industry [3]. As a result, the availability and use of mineral raw material resources makes prosperity, welfare, and a pleasant way of life for both the individual and society feasible [4]. These mineral formations, which were created by natural processes in the inner and outer portions of the earth's crust, ought to be valuable economically [5]. This makes it possible to claim that not all minerals are valuable.

On either side, valuable minerals have a connection to the metals that are used often in everyday life. When combined with oxygen, metals often yield basic oxides and have high electrical and thermal conductivity, a distinctive shine, and a strong propensity to generate cations. Gold, silver, and platinum are considered noble metals,

whereas iron, zinc, and aluminum are considered non-noble metals [6]. The characteristics of metals are best shown by full metals; semi-metals do not. Two metal and nonmetal characteristics are present in these elements. Semi-metals include elements including silicon, boron, antimony, and arsenic [7]. Metals make up the vast majority of elements in the periodic table, despite the fact that nonmetals are more prevalent in nature. Iron, aluminum, copper, zinc, magnesium, nickel, tungsten, and mercury are some of the metals that are used every day [8].

Copper (Cu) was the first metal to be worked on by humans; it was also the first metal to be discovered. The combination of tin and copper resulted in the production of a more durable bronze, which marked the beginning of the Bronze Age [9]. Copper finds its most widespread use in the construction of electrical cables and appliances due to its excellent thermal and electrical conductivity, as well as its malleability. However, there is also copper present in the equipment that is used in the industrial and building sectors. In addition, copper sulfate is used in the process of water treatment as a pesticide to eradicate algae [10]. Iron (Fe) metal is the most prevalent metal in the planet's crust and ranks as the fourth most frequent mineral that can be found on the surface of the world. Iron is the metal that sees the greatest usage overall, accounting for 95% of the weight of all metals that are produced across the globe. Because of its cheap cost in relation to its great strength, it is a vital material for use in the automobile industry, in the construction of ship hulls, and as a structural component of buildings [11]. On the other hand, steel is an alloy that is made by iron with parts of carbon, and it has a very high level of mechanical resistance as well as protection against friction. It sees widespread use in utensils, sinks, and other home appliances, as well as in commercial kitchens, food processing plants, and the automobile sector [12].

The mineral chalcopyrite is the most well-known and commonly used source of copper and iron. It is made up of $CuFeS_2$, and its density ranges from 4.1 to 4.3 grams per cubic centimeter. It is also known as faux gold due to the fact that the crystals of the substance are brittle, rice yellow in color, and have a metallic shine [13]. Pyrometallurgical and hydrometallurgical processes are used, respectively, in order to extract copper and iron from this material. In order to extract the valuable metal from the mineral using the pyrometallurgical process, the material must first undergo a

number of heat treatment the hydrometallurgical approach, on the other hand, involves dissolving the metals present in the ore and then separating them using various reagents. During the pyrometallurgical process, gases such as SO_2 and CO_2 are produced, both of which contribute to environmental concerns such as air pollution [14].

It is a well-known fact that pyrometallurgical activities have a negative impact on the surrounding environment. Despite the fact that the gases released by certain businesses are monitored, these processes nonetheless cause damage . The hydrometallurgical process should be cost-effective, capable of processing low-grade and complex ores, independently recovering each metal in high purity and not requiring high temperatures [15].

Chalcopyrite ($CuFeS_2$) is the most common copper-bearing mineral on the planet, making it crucial to the copper industry. This mineral has traditionally been processed using pyrometallurgical processes, such as in a copper smelter. The need to eliminate SO_2 emissions, H_2SO_4 marketing concerns connected with smelter operations, and the selectivity of metal extraction are driving the quest for a hydrometallurgical method as an alternative to traditional smelting to treat copper sulfide minerals. These benefits, which are mentioned for hydrometallurgical processes, are crucial elements in decision-making when environmental rules tighten and mineral processing profit margins shrink owing to lower-grade ores [16]. Chalcopyrite, on the other hand, is known to be especially resistant to hydrometallurgical operations. Despite the relatively sluggish kinetics of both chemical and biological leaching operations, there is still a lot of interest in recovering copper from chalcopyrite concentrates since it is the only source of copper in many concentrations [17].

On the other hand, the dynamics of chalcopyrite ($CuFeS_2$) leaching are well understood. A significant amount of study has been done in attempt to improve the leaching rate of this mineral, but it has not been completely effective, and the process of dissolution is still a source of debate. Because sulfide minerals are more reactive in chloride solutions than in sulfate solutions, several research of chloride systems for hydrometallurgical treatment of sulfide minerals have been conducted . A comparison

of leaching methods utilizing chloride and sulfate has revealed that the former exhibits a number of advantages when compared to the latter method. As a result, chloride leaching may be done at room temperature, but sulfate operations usually need to be done at higher temperatures. Furthermore, the copper(I) ion is stable in chloride environments, allowing copper(II) ions to be used as an oxidant alongside iron (III) [18].

For this reason, it is possible to say that the hydrometallurgical process has a significant advantage in its use in the production of metals that are extensively utilized on a daily basis, in particular copper and iron. The hydrometallurgical production of copper and iron from chalcopyrite has been the subject of a number of investigations, many of which have been deemed successful. However, these investigations did highlight a few issues that needed to be addressed[19]. These issues include things like the poor rate of copper extraction that occurs as a result of the choice of solvent reactant, and the introduction of iron into solution with copper during the extraction process. In addition, it was said that during the extraction process, the element of sulfur that is present between the crystals of chalcopyrite oxidizes and then settles on the surface of the chalcopyrite, therefore blocking the metals from entering the solution. This information was provided. In a great number of research, the issue of passivation has been tackled with the use of acids that have a high affinity for oxygen. On the other hand, there are many who believe that using this technique will result in a large rise in the cost of the extraction[20].

The passivation of chalcopyrite and the dissolution of sulfide minerals are both potential-dependent processes, and numerous research have been conducted to determine the link between the solution potential and the leaching rate. The rate of leaching in sulfate solutions is now well understood to be dependent on potential and to be improved in a certain range of potential. Many investigations have been conducted in order to determine the potentials at which dissolution and apparent passivation can occur. Conducted electrochemical and chemical studies to determine that the relevant leaching potential range is 0.45 to 0.75 V under proper experimental circumstances. However, few real dissolving investigations have been undertaken under controlled potential settings, notably in chloride [21].

Several catalysts and/or promoters have been proposed to increase the rate of chalcopyrite leaching, including pyrite, activated carbon, and the ions Ag(I), Sn(II), Co(II), Hg(II), Bi(III), and Mn (II). Some scholars have looked at the influence of pyrite on chalcopyrite leaching. Most the function of galvanic interactions in the leaching of sulfide minerals has been the subject of several of these studies. When chalcopyrite and pyrite come into close electrical contact, they create a galvanic pair, which causes chalcopyrite to serve as an anode and dissolve more quickly, while pyrite acts as a cathode and dissolves more slowly [22].

Because of its strong catalytic, thermal, electrical, and magnetic activities, the $CuFe_2O_4$ compound, which is a significant semiconductor, is utilized in a variety of applications, ranging from the treatment of wastewater to the absorption of microwave radiation. In recent years, it has been common knowledge that metal oxides with spinel structures have begun to find application as a kind of material for the storage of energy. The usage of these materials as anode electrode components in supercapacitors is by far the most widespread of these applications. Supercapacitors are devices used to store electrical energy. It works on the premise of storing energy by either providing redox reactions at the anode and cathode electrodes or absorbing ions at both of those locations[23]. Because the $CuFe_2O_4$ chemical that may be formed from chalcopyrite is capable of giving redox reactions, it has the potential to have a very high energy storage capacity for this particular application. In addition, considering that ion absorption would have an effect on the effectiveness of the energy storage, it is extremely crucial to manufacture it on the nanoscale. A supercapacitor's electrodes are made up of a current collector that is conductive as well as a coating that is applied to the surface of the collector. Nickel foam is by far the most typical kind of current collector that is used for this function. The hydrothermal technique is capable of being used in the production of a metal oxide on the surface of nickel foam. One example of this is $CuFe_2O_4$, which may be obtained via the process. This method's overarching goal is to produce nanoparticles by synthesizing them from salts that have been dissolved in a liquid phase medium. The most significant benefit is that the synthesis may be carried out at lower temperatures, which is also one of the advantages. For this reason, it is feasible to synthesis $CuFe_2O_4$ compound on the surface of nickel foam by

the hydrothermal process in nano size so that it may be used as an anode electrode in supercapacitors.

In consideration of each one of these hypotheses, the primary objective of my research for my thesis is to investigate the ways in which varying concentrations of HCl, HNO_3, H_2SO_4 influence the process of extracting copper and iron from chalcopyrite. In order to accomplish this goal, the concentrations of copper and iron in the solutions that were produced following the extraction operations were measured using atomic absorption, and the findings were assessed. After that, the solution with the greatest concentration was chosen, and on the surface of the nickel foam using the hydrothermal process, $CuFe_2O_4$ was manufactured using this solution. Analyses using FTIR, XRD, and SEM were used in order to determine the chemical bonding, crystalline structure, and microstructure of the products that were produced. After that, electrochemical characterization was performed using galvanostatic charge-discharge (GCD) measurements in a three-electrode setup to use as a supercapacitor electrode. As a consequence of these findings, the specific capacitance, energy, and power densities of the electrode that was created were estimated. After that, the data that were produced were compared with the studies that were already published in the relevant literature. As a consequence of this, details on the benefits, drawbacks, and significance of this research are discussed in relation to the existing body of previous work.

PART 2

EXTRACTION

2.1. COPPER

Copper, with the atomic number 29, is one of the earliest metals used by humans, having been used for coinage and ornaments in Western Asia for at least 10,000 years. Copper has played an important role in the evolution of human civilization since the prehistoric Chalcolithic Period and Bronze Age. Great scientists like Ampere, Faraday, and Ohm made breakthroughs in electricity and magnetism in the late 18th and early 19th centuries, which aided the industrial revolution and catapulted the copper industry into a new era. Copper continues to play a vital role in our modern lives, and new applications for the metal are being created all the time [24]. Copper's electrical and thermal conductivity (surpassed only by silver), great ductility and consequently excellent workability, and corrosion resistance (a chemical behavior that makes it a half noble metal) are all important physical and chemical qualities. Copper is now utilized in a variety of products, including electrical power cables, data cables, electrical equipment, vehicle radiators, cooling and refrigeration tubes, heat exchangers, artillery round casings, small arms ammunition, water pipes, and jewelry. Copper is the 26th most plentiful metal [25].

Copper is the 26th most abundant element in the earth's accessible sphere, with an average concentration of 50 parts per million. It can be found in over 200 minerals, although only around 20 of them are useful as copper ores. The most important copper minerals and their copper concentration are summarized in Table 2.1 [26]. Copper is a chalcophilic element, hence the most common minerals are sulfides like chalcopyrite and bornite. Although there is no current information on chalcopyrite reserves, it is known that chalcopyrite accounts for nearly half of all known copper. Porphyry ore deposits provide the majority of the copper produced worldwide [27]. The major

sulfides (chalcopyrite and bornite) are found at the deepest level of a typical porphyry ore deposit. Secondary minerals originate in two stages near the earth's surface. Copper oxides, sub-carbonates, and sub-sulphates are formed in the upper section (the oxidation zone) by oxygen-containing water. Copper bearing solution from the oxidation zone is changed into secondary copper sulfides, chalcocite and covellite, in the deeper cementation zone, above the main sulfide zone [28].

Table 2.1. The most important copper minerals

Type	Minerals	Formula	%Cu
Primary Sulfide minerals			
Hypogene Sulfides	Chalcopyrite	$CuFeS_2$	34.6
	Bornite	Cu_5FeS_4	63.3
Secondary minerals			
Supergene Sulfides	Chalcocite	Cu_2S	79.9
	Covellite	CuS	66.5
	Digenite	$Cu_{18}S$	78.1
Native copper	Metal	Cu	100.0
Carbonates	Malachite	$CuCO_3+Cu(OH)_2$	57.5
	Azurite	$(CuCO_3)_2+Cu(OH)_2$	55.3
Hydroxy-silicates	Chrysocola	$CuO+SiO_2+ 2H_2O$	36.2
Oxides	Cuprite	Cu_2O	88.8
	Tenorite	CuO	79.9
Sulphates	Antlerite	$CuSO_4+2Cu(OH)_2$	53.7
	Brochantite	$CuSO_4+3Cu(OH)_2$	56.2

For copper production, open pit mining is the most common method. Copper is mostly manufactured via pyrometallurgical processes, which include roasting, smelting, and refining. According to the International Copper Study Group (ICSG), pyrometallurgical processes produced roughly 60% of all copper in 2012. Aside from that, copper scrap treatment, which is mainly pyrometallurgical, accounted for 18% of global production. However, as the global demand for copper grows and the average quality of mined ores declines, hydrometallurgical technologies for the efficient processing of low-grade ores and wastes have become more popular in recent years. In 2012, hydrometallurgical processes accounted for 22% of total copper production. A brief summary of pyrometallurgical and hydrometallurgical processes is provided in the following sections [29].

2.2. COPPER MINERALS

Copper (Cu) is a versatile industrial metal that is both ductile (able to be pulled into wire) and malleable (able to be hammered and molded) as well as a good conductor of electricity (only silver is better). Copper may be found in a variety of minerals that can be mined. Azurite, malachite, chalcocite, Bornite , chrysocolla, cuprite, are some examples of these minerals. Chalcopyrite supplies the majority of copper [30].

Azurite: $Cu_3(CO_3)_2(OH)_2$ is the chemical formula for azurite, a copper carbonate hydroxide mineral. It is most well-known for its deep blue to violet-blue hue. The deep blue evening sky typically seen over deserts and winter landscapes are reminiscent of the "azure" color. Although azurite is not a common or plentiful mineral, it is attractive due to its blue hue. It has been utilized for thousands of years by people all across the world. It was utilized as a copper ore, a pigment, a gemstone, and a decorative stone by the ancients. Today, it's still used for all of these things [31].

Malachite: Malachite, a green copper carbonate hydroxide mineral having the chemical formula $Cu_2(CO_3)(OH)_2$, is a green copper carbonate hydroxide mineral. One of the first ores utilized to make copper metal was this one. Because it is generally discovered in tiny quantities and may be sold for better rates for other sorts of usage, it is of minimal value as a copper ore today. For thousands of years, malachite has been utilized as a gemstone and sculptural material, and it remains popular today. Today, it's most commonly used in jewelry as cabochons or beads. The green tint of malachite does not fade with time or exposure to light. These characteristics, combined with its ease of grinding to a powder, have made malachite a popular pigment and coloring ingredient for thousands of years [32].

Chalcocite: Chalcocite (from the Greek chalcos, "copper") is a significant copper mineral, with 79.8 parts per hundred of the native elements when pure. It may be found in hydrothermal veins, copper deposits, and the cementation zone of such deposits. Pyrite, chalcopyrite, cuprite, quartz, azurite, malachite, calcite, and bornite are all found in its vicinity. It's also mined in sedimentary deposits, where leaching

accumulates it. Chalcocite is a mineral that is soluble in nitric acid (HNO_3) and lends a green hue to the flame [33].

Bornite: Bornite is a Cu_5FeS_4 copper iron sulfide mineral. It can be found in rocks that are igneous, metamorphic, or sedimentary. Bornite is found in hydrothermal veins, contact metamorphic zones, and the enriched zone of numerous sulfide mineral occurrences in mineable concentrations. Bornite is frequently linked with chalcopyrite, marcasite, and pyrite, which are all sulfide minerals. Bornite is also found in mafic igneous rocks and carbonaceous shales in small levels [34].

Chrysocolla : hydroxylate appears as glassy botryoidal or spherical masses or bubbly crusts, as well as jackstraw mats of small acicular crystals or tufts of fibrous crystals and is usually linked with other secondary copper minerals. Chrysocolla crystals have never been discovered. The "crystals" of chrysocolla are all pseudomorphs. Copper-bearing allophone can have a similar appearance [35].

Cuprite : this oxide CU_2O is frequently found in the top zones of veins as an oxidation result of copper sulfides, and is frequently associated with Native Copper, Malachite, Azurite, Limonite, and Chalcocite. Chalcotrichite is a fibrous variety of Cuprite [36].

Antlerite : In dry locations, a secondary mineral found in the oxidized zone of copper deposits. It's less frequent than brochantite, a related and occasionally superficially similar mineral with which it's sometimes mistaken. In comparison to brochantite, metastable at room temperature; seems to develop at higher temperatures (60-80°C) [37].

2.2.1. Chalcopyrite Minerals

Copper ore is the 25th most prevalent element on earth and occurs in the crust of the earth at a rate of around 0.01% on average. As a result of liquid penetrating the magma layer and making its way into the crust of the earth, heavy metal sulfides were broken down. It is thought that the most prevalent kind of copper mineral, chalcopyrite, which consists of $CuFeS_2$ and 34.6% copper, developed in this manner as a primary mineral

(primary). Conversely, sulfide minerals may undergo oxidation and reduction by the chemical influence of hot natural vapors or leaky sulfate solutions to produce secondary (secondary) oxidized copper minerals and metallic copper (native copper). As the higher oxidized copper minerals are extracted from numerous mineral sources, sulfide copper ores are eventually obtained as a result. Sulfide minerals make up around 85 percent of the world's known copper ores, whereas oxide minerals make up 15 percent [38]. Bornite (Cu_5FeS_4), chalcopyrite ($CuFeS_2$), chalcocite (Cu_2S), and covellite (CuS), as well as enargite (Cu_2 (As, Sb)S_4), are the sulfide ores that are considered to be the most important. On the other hand, oxidized forms of copper ores may be found in the form of sulfates, carbonates, and silicates. Malachite [$CuCO_3Cu(OH)_2$], Chrysocolla [$CuSiO_{32}H_2O$], azurite [$2CuCO_3Cu(OH)_2$], brochantite [$Cu_4SO_4(OH)_6$], cuprite [Cu_2O], tenorite [CuO], and malachite [$CuCO_3Cu(OH)_2$] are all examples of significant oxidized copper ores [39].

The mineral known as chalcopyrite has the formula $CuFeS_2$ as its chemical composition, and its molecular weight is 183.53 grams [40]. Its composition reveals that it has 30.43% iron, 34.63% copper, and 34.94% sulfur. It is most often discovered in dispersed volcanic rocks as well as sulfide veins. Figure 2.1. [41]. Illustrates the crystal's shape and reveals that the crystal system in question is tetragonal. In this particular crystal lattice, Co, Ni, Mn, Zn, Ag, Au, Pb, and Cr may be replaced by Fe and Cu, while S can be replaced by Se and Te. Therefore, chalcopyrite ores might potentially include a wide variety of valuable and nonprecious metals and nonmetals. It has a metallic shine, an orange-yellowish hue, a stripe color that is greenish-black, a density of 4.28 grams per cubic centimeter, and a Mohs hardness of 3.5-4.

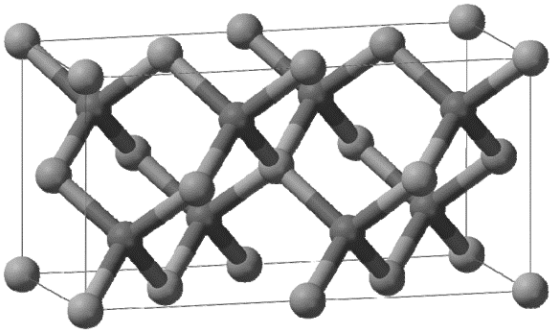

Figure 2.1. Chalcopyrite unitcell (Cu: red, Fe: blue and S: yellow coloured) [41].

2.2.2. Dissolution Process of Chalcopyrite

Copper oxide minerals (including chalcopyrite) dissolve more easily than sulphides due to their chemistry. The rationale can be found Pourbaix diagram of a Cu-S-OH_2O system in figure. 2.2. Copper oxides' stability area is already in the diagram's greater oxidation potential zones. As a result, simply lowering the pH (with an acid) is enough to dissolve copper from oxide minerals.

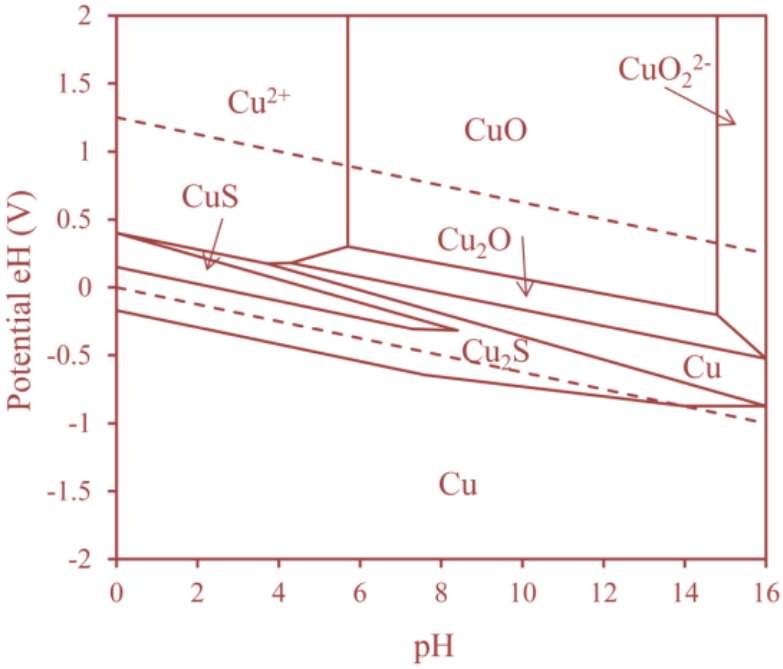

Figure 2.2. Pourbaix diagram of a Cu-S-O-H_2O system

In the event of direct leaching, the use of appropriate oxidizing solvents is required, despite the fact that such calcined materials may be readily leached with acids or solvents that complicate matter. Sulfate, chloride, nitrate, ammonia, and biological systems are all viable options for use in leaching sulfide copper ores [42]. The leaching of chalcopyrite concentrate may be accomplished using sulfuric acid solution in two stages. The first of these processes involves converting the sulfides present in the ore to sulfate using acid at a temperature between 220-230 degrees Celsius, after which the sulfate is diluted with water and leached [43]. The equations 2.1, 2.2, 2.3, and 2.4 below show the reaction steps that need to take place in order to complete this procedure [44].

$$CuFeS_2 + 2H_2SO_4 = CuSO_4 + FeSO_4 + 2H_2S \quad (2.1)$$

$$H_2S + H_2SO_4 = S° + SO_2 + 2H_2O \quad (2.2)$$

$$2FeSO_4 + 2H_2SO_4 = Fe_2(SO_4)_3SO_2 + 2H_2O \quad (2.3)$$

$$CuFeS_2 + 2H_2SO_4 + O_2 = CuSO_4 + FeSO_4 + 2SO + 2H_2O \quad (2.4)$$

On the other hand, the chalcopyrite ore may be dissolved when sulfuric acid and oxygen are present in a solution of a more diluted concentration. Ozone is often used in place of oxygen in scientific experiments. Many hydrometallurgical processes have been developed in response to this situation. Cymet, CLEAR, Sherritt Gordon Cominco, H_2SO_4 - pressure in the presence of oxygen, and ammonia pressure leaching in the presence of oxygen are the primary mechanisms that are in concern [45].

Chalcopyrite concentrates are processed hydrometallurgical using chloride in the CLEAR (Copper Leaching, Electro winning, and Recycle) process [46]. The Duval Corporation is responsible for developing this method. Two steps of leaching are included in this process, which was created by. In the first step, chalcopyrite is produced by adding 20 g/L of acidic $CuCl_2$ to a solution that contains 4 g/L of $FeCl_3$. This step is performed at a temperature of 105 °C. Copper with a valence of $^{+2}$ is changed into copper with a valence of Cu^+ during the second step of the process, which sees the addition of metallic copper to the solution that was produced in the first stage. After that, the solids and liquids are separated from one another. Electrolysis is the procedure that is used in order to extract copper from the clear solution that was produced. In order to dissolve the chalcopyrite that could not be brought into solution in the first stage, the leaching sludge is leached in a solution that contains 44 g/L of KCl. The temperature is set at 150 degrees Celsius, and the oxygen partial pressure is set at 50 pounds per square inch. Because of the high temperature and the high pressure of the oxygen, part of the sulfur changes into sulfate and precipitates as potassium jarosite, which has the chemical formula $KFe_3(OH)6(SO_4)_2$. The fundamental reactions that took place in this situation are outlined in the equations 2.5, 2.6, 2.7, and 2.8 and 2.9 [47].

$$CuFeS_2 + 3CuCI^+ + 11Cl^- = 4CuCl_3^{-2} + FeCl_2 + SO \quad (2.5)$$

$$Cu + CuCl + 5Cl^{-} = 2CuCl_3^{-2} \quad (2.6)$$

$$CuFeS_2 + FeCl_2 + 3/2O_2 + 3H_2O = CuCl_2 + 2Fe(OH)_3 + 2SO \quad (2.7)$$

$$CuCl_3^{-2} + e- = Cu^{+3}Cl^{-} \quad (2.8)$$

$$CuCl_3^{-2} = CuCI^{+} + e^{-} \quad (2.9)$$

$$6FeSO_4 + 12FeCl_2 + 9/2O_2 + 3KCl + 9H_2O = 3KFe_3\,(SO_4)_2(OH)_6 + 9FeCl_3 \quad (2.10)$$

The Sherritt Gordon process is a technique used in industry that involves leaching sulfide copper minerals with ammonia while the mixture is under pressure. The creation of the $Cu(NH_3)_{4\,+2}$ complex is the fundamental step in this process. In order to treat the Ni, Cu, and Co complex ore that comes from the Lynn Lake mine in Canada, it was designed [48]. Since 1954, this well-established factory has been consistently turning out products. In this process, a solution containing concentrated ammonia and ammonium sulfate is mixed together and then leached at a temperature of 85 degrees Celsius while oxygen pressure is applied. Distillation is used to remove some of the free ammonia that is present in the leach solution. At a temperature of 250 degrees Celsius and a pressure of 27 atmospheres, some of the sulfur compounds in solution are oxidized to become sulfate compounds. Copper is recovered by first neutralizing the free ammonia with sulfuric acid and then precipitating it with hydrogen at temperatures of 200 degrees Celsius and 40 atmospheres of pressure.

The Sherritt Gordon approach and the Arbiter method are comparable in many respects. In the Arbiter process, oxygen is used rather than air, and it is not necessary to work at high pressures. Ion exchangers are used in this approach rather than the Sherritt Gordon method in order to remove copper from the solution [49]. This is yet another key distinction between the two processes. When using the Arbiter approach, the dissolutions of the various copper minerals were represented by the equations 2.11, 2.12, and 2.13.

$$CuS + 4NH_3 + 2O_2 = Cu(NH_3)_4SO_4 \quad (2.11)$$

$$Cu_2S + 4NH_3 + (NH_4)_2SO_4 + 5/2\ O_2 = Cu(NH_3)_4SO_4 + H_2O \quad (2.12)$$

$$2CuFeS_2 + 6\ NH_3 + 17/2\ O_2 + (n+2)H_2O$$
$$= 2Cu(NH_3)_4SO_4 + 2(NH_4)_2SO_4 + Fe_2O_3.nH_2O \quad (2.13)$$

2.2.3. Passivation Problems of Chalcopyrite

Several investigations have found that chalcopyrite leaching rates decrease with time and eventually stop, implying that dissolution is slowed by the creation of a passivating layer. Passivation occurs in the potential zone associated with oxidative dissolution, according to electrochemical studies, and is caused by the creation of a surface layer that prevents dissolution [50]. Passivation occurs at a critical potential that is regulated by chloride concentration, temperature, and the presence of certain contaminants, according to new research. The nature of the passivating layer and the conditions under which it forms has been the subject of numerous investigations. It is still probably the most contentious component of chalcopyrite leaching. As a result, several theories concerning the reason of passivation have been proposed, including the production of a Sulphur layer. A polysulfide or metal-deficient layer, and even iron complexes that have precipitated [51] .

Despite the fact that elemental sulfur is generated during leaching, there is ongoing debate among scientists as to whether sulfur is the primary source of passivation. Only elemental sulfur is generated during ferric chloride leaching of chalcopyrite, and no intermediary phase between elemental Sulphur and chalcopyrite is seen. Chalcopyrite residues treated with acid ferric and ferrous sulfate and chloride solutions and found that elemental Sulphur and disulphide surfaces were formed the use of X-Ray photoelectron spectroscopy (XPS), secondary ion spectrometry (TOF-SIMS), and scanning electron microscopy (SEM) to study the surface layers of a chalcopyrite surface leached in perchloric acid. There are three stages to chalcopyrite leaching. Polymerization of S^{-2} to polysulfide Sn^{-2} happens first, followed by reformation of S^{-2} and other chain polysulfides, which recrystallize with additional oxidation to create crystalline sulfur [52].

Intermediate sulfur layer covellite (CuS) was found as an intermediate product in the anodic dissolution of chalcopyrite researchers. The production of a product layer comprised of covellite and elemental sulfur. CuS dissolves and reformed in the pores of elemental sulfur, preventing further dissolution. Parker et al. (1981) discovered that when chalcopyrite was oxidized at 0.4 V in acidic chloride solutions, blue covellite developed on the surface. CuS might be a byproduct of $CuCl_2$- sulfur reactions or a byproduct of non-oxidative processes involving the synthesis of CuS. The acid HCl solutions include H_2S. The copper sulphides in anodic stripping curves, but conceded that confirming CuS as the result was challenging, and the only proof of CuS was the presence of a few blue spots on a chalcopyrite surface seen microscopically [53].

Polysulfide layer it would seem that the production of the sulfur layer is not consistent, since it displays discontinuities that have been linked to the presence of cycles of peeling and formation in sulfate media. as a result of the precipitation of sulfur granules onto mineral particles, which was formed via the oxidation of the chalcopyrite by-product H_2S by ferric iron in solution. An increase in the roughness of the particle has been shown to occur under the sulfur layer in sulfate and chloride environments. This results in an increase in surface area, which works against the process of passivation through diffusion. This impact may be able to overcome the inhibition of leaching caused by diffusion in chloride media as a consequence of the increased porosity, which is what gives rise to the linear kinetics that is seen [54].

2.3. PYROMETALLURGICAL METHODS

The ore is crushed and pulverized once it is mined. Flotation concentrates the ground ore into a finished product that typically contains 20-30% copper (for chalcopyrite concentrate). The dried concentrate, mixed with silica and flux (as slag former), is fed to the flash smelter, where partial roasting and smelting occur concurrently, as shown in figure 2.3. Oxidation reactions yield Sulphur dioxide gas. This gas is caught and utilized to manufacture sulfuric acid. In the flash furnace, liquid matte and slag separate at roughly 1200° C [55].The matte is tapped and sent to the converter for ultimate conversion of copper sulfide to elemental copper, which comprises 50-70

percent copper primarily as sulfide. After the converter, the result is known as blister copper, and it contains roughly 98-99 percent copper. The blister copper is then fire refined to remove any leftover oxygen before being cast into anodes for electrorefining [56]. Electrorefining produces copper cathodes that contain over 99.99 percent copper other units for treating anode slimes containing valuable metals, as well as units for treating scraps, may be added to this flow-sheet.

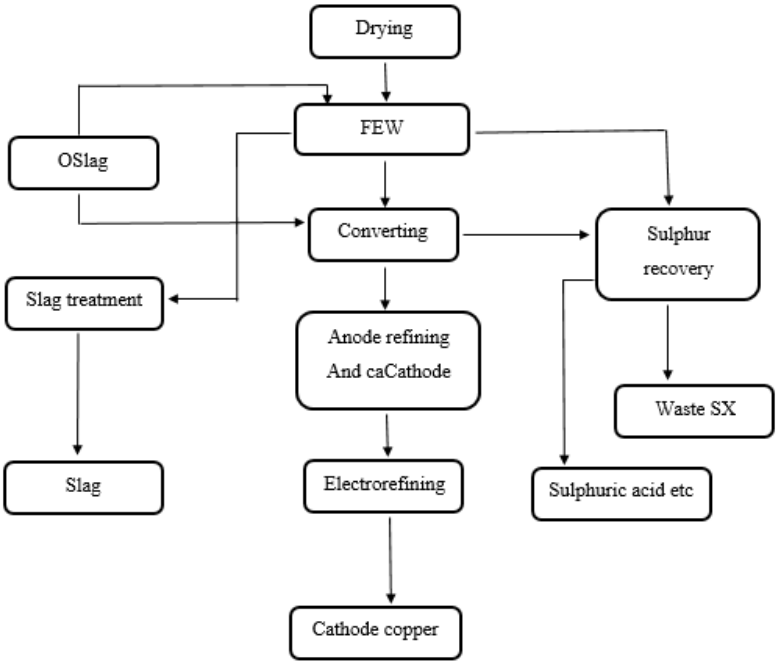

Figure 2.3. A typical pyrometallurgical flow-sheet for copper production [57].

2.4. HYDROMETALLURGICAL METHODS

Hydrometallurgy is a kind of extractive metallurgy that makes use of liquid chemical solutions [45]. The goal is to extract value from ore by purifying it or recycling the valuable metals that were extracted. Leaching, purification, and metal recovery are three categories that may be used to analyze the process. Recovering precious metals by leaching involves employing solvent-containing liquid chemicals. Chemicals (typically an acid or a base) are used to dissolve the metal to be enhanced, and then the solution is collected. The characteristics of the metal being dissolved may dictate the kind and concentration of the chosen chemicals. Modifications in pH, temperature,

and oxidation potential may all influence how well leaching works. It is possible that additional metals in the ore were also dissolved during the leaching process [48]. A simplified hydrometallurgical flow-sheet for copper extraction is shown in figure 2.4.

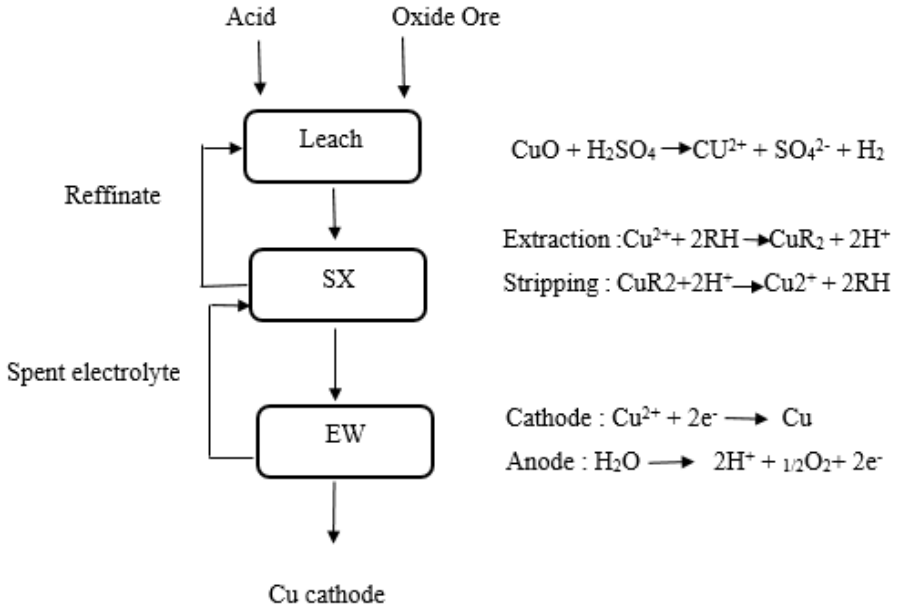

Figure 2.4. Simplified copper production from oxide ores [57].

Copper is solubilized from the ore in the leaching stage by a lixiviant, which commonly comprises sulfuric acid. Sulfide mineral leaching also requires the presence of oxidizing agents like ferric ion and oxygen. Apart from copper, numerous other elements (such as Fe, Al, Co, Mn, Zn, Mg, and Ca) are leached into the solution during the leaching stage. With a copper content of 1-10 g/L, pregnant leaching solution (PLS) advances to SX. The PLS is combined with an organic solvent containing a Cu-specific organic extractant during SX (RH) [58]. All other contaminants in the aqueous phase are left behind as copper is selectively placed on the extractant. Raffinate, a barren aqueous phase, is returned to the leaching stage and employed as the lixiviant. A strong sulfuric acid solution, which is the wasted electrolyte from EW, is subsequently used to extract copper from the loaded organic phase [59]. After stripping, the solution contains roughly 45 g/L copper and moves on to the EW step. The organic solvent is removed and reintroduced to the extraction step. Finally, copper is plated on cathodes after being reduced by a DC current in EW. The impurity of copper cathodes is normally less than 20 ppm.

PART 3

NANOTECHNOLOGY AND ENERGY DEPOSITION

3.1. NANOPARTICLE SYNTHESIS METHODS

By working at the level of atoms and molecules (in the range of 1 to 100 nm in units per billion), nanotechnology is the construction of structures with better and/or totally new physical, chemical, and biological quality. In general, the material characteristics and operating principles of the devices are based on conventional modeling and theory (assumptions based on dimensions bigger than 100 nm) [60]. This is because conventional modeling and theory are the most accurate representations of the physical world [61]. However, when the dimensions are lowered to less than 100 nanometers, conventional theories and models are unable to adequately describe the newly appearing properties. Nanomaterials, which are very small particles of the same substance, display better and unique features as compared to larger particles of the same material. There is a diverse assortment of nanomaterials and particles that may be discovered in their natural state on Earth. Some examples of these are photochemical compounds, volcanic products, and exhaust gases [62]. The primary objective of nanotechnology is to facilitate the creation of products that are more durable, of higher quality, have a longer lifespan, are more affordable, lighter, and smaller. Because of this motivation, several nanoscale manufacturing technologies are now being development. These are discussed in further depth in the next section. In addition, the usage of nanoparticles that can be manufactured for the purpose of this use in supercapacitors as well as their characterization are both discussed in the sub-titles [63].

Top-down production and bottom-up production are the two primary strategies that may be used in the manufacturing of nanomaterials and structures [64].In the first method, known as the top-down method, the procedure begins with the whole content, which is then cut up into manageable chunks. This method is also referred to as the "bottom-up" method. Using lithography, exceptionally perfect surface shaping, specific processing processes, and chemical etching methods, this primary method brings the structural dimensions of minuscule components down to the nanoscale scale. The bottom-up manufacturing method involves the synthesis of the material as a consequence of the development in size of atoms and molecules brought about by chemical processes [65]. In order to create bigger systems, clusters, organic lattices, multimolecular structures, and synthetic macromolecules, atomic and molecular constituents are brought together in a way that is under controlled conditions. These may be broken down into three categories: techniques of synthesis that take place in solid phase, liquid phase, and gas phase [66].

3.1.1. Vapor Phase Synthesis

Because it is able to give flexibility and regulated material production, the inert gas condensation technique is one of the most preferred methods for the manufacture of nanoparticles [67]. Evaporating the beginning material in the presence of a pure helium environment and then cooling the vapor that is generated in the presence of the helium atmosphere are the two steps that make up the method's core operating principle. The next step, which is the condensation of atoms into nano particles, comes after this process. The nano particles that are created as a consequence of this process are then transported and gathered in the collector. Small, condensed particles are transported into the collecting jar by convection currents, which are heated by the inert gas and chilled by the cold finger. After being scraped, the deposits are sent to the compression apparatus. The created particles have a size that ranges from one to one hundred nanometers, and one may vary the size of the produced particles by modifying the gas pressure. After that, the gathered particles might be sintered, in order to produce solid nanomaterials, if that is required. The gas pressure, the kind of inert gas, the temperature, and the gas flow rate are the primary factors that have an effect on the system as well as the characteristics of the product [68].

Physical Vapor Deposition, sometimes known as PVD, is a technique that coats material from a solid or liquid source by means of vapor convection and condensation (typically in a vacuum environment) [69]. As long as the circumstances of the process are meticulously managed, this approach may produce thin films with dimensions as small as an atom or as large as a nanometer. This method is a diverse manufacturing method. Evaporation, sputtering, laser heating, or ion beam are all examples of vapor phase types that may be created by the process of PVD [70]. When using sputtering, atoms are separated from the surface of the target by the impact of ions, but when using evaporation, atoms are removed from the source using thermal methods. After the resultant vapor phase goes through the stages of collision and ionization, the substrate begins to concentrate on the sample, which is then followed by the processes of nucleation and growth. Sputtering is also used to build layers of materials with high melting temperatures, such as refractory metals and ceramics, which are very difficult to make by thermal evaporation. These layers may then be employed in a variety of applications. Sputter-formed films typically have a greater density than evaporation-formed films due to the fact that sputtering atoms carry more energy than evaporating atoms. The capacity of PVD methods to generate thick films at very low substrate temperatures and their rapid film growth rates are two of the primary benefits of using these technologies [71].

The chemical vapor deposition technique, also known as the CVD method, was first developed in Germany in 1994. It is a process that is appropriate for the manufacture of a huge quantity of nanoparticles [72]. The process entails the transformation of gaseous material into particles by thermal cracking. This is the fundamental concept behind the procedure. At the nanoscale, chemical vapor deposition (CVD) is a manufacturing process that is commonly utilized. Its primary function is to apply a thin film coating to the surface, but it is also put to use in the manufacturing of high-purity bulk materials and powders [73]. This is the most common application for its usage. During the CVD process, gaseous or vaporous raw materials are transferred onto the heated substrate, where they either react chemically or serve as a transport medium for other raw materials. On or near heated surfaces, reactions take place, and the resulting solid products are deposited on the surface in the form of thin films. Using this approach, it is feasible to produce a large range of different types of materials. The

CVD process utilizes a wide variety of different kinds of reactors. They are categorized as either having hot walls or cold walls, being either low pressure, atmospheric pressure, or high pressure, and having carrier gas or not having carrier gas. Temperatures ranging from 473 to 1873 K are acceptable for carrying out deposition procedures inside these reactors. At the same time, chemical vapor deposition (CVD) techniques may be separated into many categories based on the kind of energy source (plasma, photon, laser, or hot filament) that is used. The CVD procedure offers a wide variety of benefits. On intricately shaped components, it can often produce a homogenous thick film or coating layer, which is one of the most significant benefits of the process. The ability of the CVD technique to facilitate the synthesis of materials of very high purity is another one of its many benefits. Other benefits include relatively high deposition rates and a general need for a vacuum that is often lower than that needed for the PVD process [74].

3.1.2. Liquid Phase Synthesis

The mechanism that results in the creation of particles in the vapor phase process is also present in the liquid phase process. Although grain size and crystal form are not simple to manage in normal gas condensation, it is possible to keep these qualities under control by the use of growth-limiting organic ligands in sol-gel and solvothermal synthesis. The processes of nucleation, growth, and/or agglomeration may all take place concurrently during chemical precipitation (CP) reactions. The circumstances of super saturation are often necessary for the formation of insoluble particles. The nucleation stage is the most important step since it is when a significant number of minute particles are produced. On the other hand, secondary processes like maturation or aggregation have a substantial impact on the final product's size, shape, and characteristics after they have been completed [75]. It is necessary to achieve super saturation (saturated), which often takes place as a consequence of a chemical reaction, in order to make the precipitation process easier. The synthesis of metals (from aqueous solutions, reduction from non-aqueous solutions, electrochemical reduction, and degradation of metal-organic precursors) as well as oxides (from both aqueous and non-aqueous solutions) and metal precursors are examples of typical chemical precipitation processes (by reactions of molecular precursors). In addition to this,

chemical precipitation techniques using microwaves and sonication may also be used [76].

Another example of a wet-chemical procedure is the sol-gel process. During this procedure, a network structure known as a gel is generated by utilizing either a chemical solution known as a solvent solution or colloidal particles known as a sol for nanoscale particles [77]. The procedure begins with the preparation of a stable sol that contains solid particles in solution, and it is then followed by a gelling reaction that is either a polycondensation or a politzerization reaction. The liquid phase that the gel once had is extracted via drying it. In the last stage of the process, a high temperature is used to densify (densify) and decompose the gels. During this time, the gel precipitates in the form of pores in the network structure, and any remaining organic impurities are eliminated [78]. Gel is the linked network that forms between phases, whereas sol is a colloidal suspension of solid particles in a liquid phase. Sol may be thought of as a kind of gel. Instead of producing particulate metallic sols, both processes result in the production of polymeric sols (which are free of oxide particles bigger than 1 nm). Both of these reactions are multi-step processes that take place in the order listed. Precursors for sol-gel materials may take the form of metal alkoxides, as well as inorganic and organic salts. Many different kinds of research are conducted using metal (Si, Ti, Zr, Al, and B) alkoxide precursors [79].

Hydrothermal synthesis is considered to be one of the most effective ways for the production of pure metal oxide nanoparticles. By using a heterogeneous reaction under circumstances of high temperature and high pressure, this technique allows for the growth of compounds that are incapable of solubility under conditions of normal temperature and pressure. The process of growing crystals takes place in a device known as an autoclave, which is made up of a steel pressure vessel. Inside of this device, the water and the nutrients are kept together. Hydrothermal synthesis allows for the production of materials that are not able to be created by reactions that take place in solid state. After this step, you will get the final product, which typically has a low melting point, a high vapor pressure, and undergoes thermal breakdown. It is simple to make goods in the intermediate state, the meta-stable state, and certain phases, and it is also possible to synthesis new meta-stable state chemicals and other

compounds in certain condensed states. The most significant drawbacks of hydrothermal synthesis are the need for the use of pricey autoclaves, the presence of potential safety issues during the reaction process, and the absence of any means by which the reaction may be seen [80].

3.1.3 Synthesis in the Solid Phase

Grinding by Mechanical Means The process of mechanical etching is a good example of a "top-down" approach that is used in the synthesis of nanomaterials. Mechanical grinding also falls into this category. This technique does not include the production of the nanomaterial from clusters; rather, it relies on the structural deterioration of coarse particles that have been created as a consequence of plastic deformation. The mechanical grinding of materials is a common practice since it is uncomplicated, does not call for any costly machinery, and is an effective technique for producing materials of various grades, including nanocrystalline materials. In actual practice, it is essential to pay close attention to the contamination that may originate from the atmosphere or environment in which the grinding is taking place, as well as the consolidation of the powder product into a nanocrystalline microstructure without any coarsening. In the process of mechanical grinding, high-energy mixers, spherical balls, or tumbler mills may be used. There is a transfer of energy from the refractor or the balls to the powder material. The amount of energy transferred is dependent on the number of balls, the rotating speed, the size, the ball/powder mass, the grinding period, and the environment in which the grinding takes place. This technique of synthesis is well-suited for the creation of amorphous or nano-crystalline alloy particle powders, as well as elemental or compound powders [81].

3.2 THE ENERGY STORAGE SYSTEM AND SUPERCAPACITORS

Dependence on fossil fuels has caused significant issues for contemporary society, including rising fuel prices, pollution, climate change, and geopolitical tensions [82]. Other energy sources and storage technologies have been among the major focuses of governments as they work to mitigate these issues on a worldwide scale. The setting has prompted a wealth of research into the potential of renewable energy sources such

wind, solar, biomass, hydrogen, geothermal, and hydrothermal [83]. Indeed, the electrical energies derived from these investigations find widespread use in many aspects of our everyday lives. Although their power production is not consistent, these sources may be found in nature and transform kinetic energy into electricity. So, it's crucial not only to get energy, but to store it and have it ready to go with the right outputs when they're required. Up to now, energy storage devices known as capacitors have been utilized here [84]. Devices of this kind are created by inserting an insulating substance between two conducting surfaces. In this setup, current attempts to flow through the insulator when a source voltage is put between the capacitor's plates, but the insulator acts as a barrier to the passage of electrons. Energy may be stored in a dielectric substance as an electrical field thanks to a phenomenon called resistance. So, the plates store energy by being charged in different directions yet at the same time[85]. The value of its capacitance is proportional to the dielectric constant of the substance that fills the space between the plates. This data suggests that sandwiching components with a high dielectric constant between metal plates yields a high capacitance value. Components having a perovskite structure and a high dielectric constant, such $BaTiO_3$ and $SrTiO_3$, have been reported to provide very high capacitance in this setting [86]. In addition, many electronic devices make use of polymers such polyaniline, PVDF, and metal oxides because of their high capacitance value [87]. Recent advances in technology, however, need not just more greatly power output, but also greater energy density and a shorter charge-discharge cycle time. Instead of employing materials with a high dielectric constant, Helmholtz believed that a greater energy storage capacity might be attained by lowering the thickness of the dielectric material between the plates and increasing the surface area [88].

To achieve this, double layer super capacitors (Figure 3.1) have been created [89]. These consist of a conductor with a higher dielectric surface area, a liquid electrolyte for ion exchange, and a separator that enables ions to pass. While the supercapacitor is being charged, the electrodes get populated by the electrolyte's negatively and positively charged ions. Meanwhile, the size of the ions in the electrolyte is exactly equal to the thickness of the dielectric material at the interface (1 nm). This thickness may often be lowered to between 2 and 5 m in traditional capacitors. The increase in capacitance is almost a factor of a thousand even when just the thickness value is

considered. As a result, supercapacitors have a greater energy storage capacity than regular capacitors.

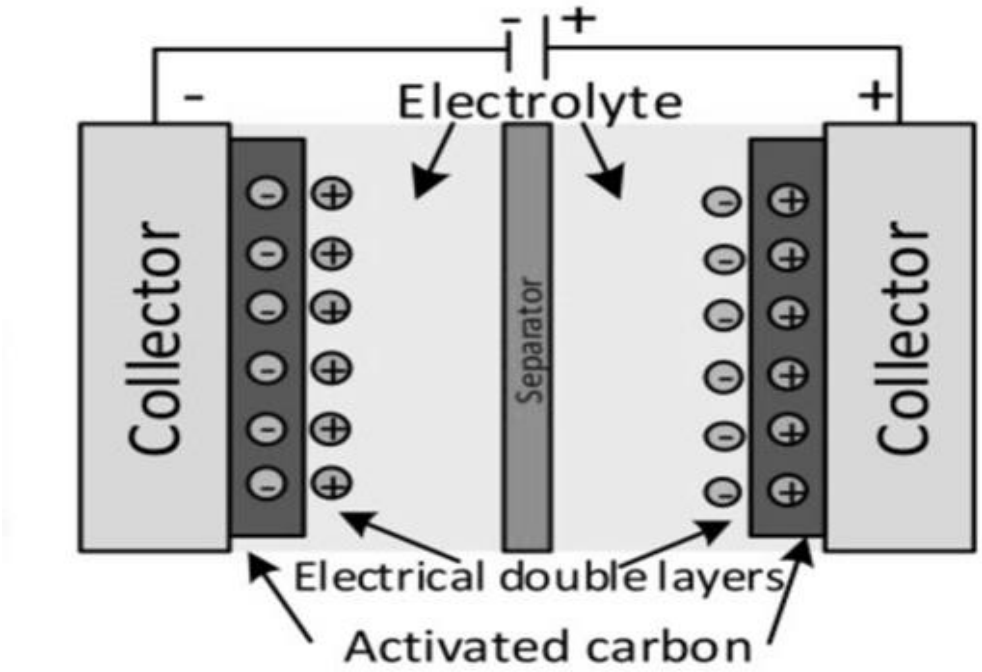

Figure 3.1. Schematic representation of porous supercapacitor electrode [90].

Charges may be stored on the surface and near the surface of these types of supercapacitors by a process called adsorption, as well as through faradic processes, which include the creation of redox reactions on the surface. This kind of capacitor is known as a pseudo capacitor [91]. There is also a sort of hybrid supercapacitor that can store energy in both a double-layer and a pseudocapacitive fashion simultaneously. Hybrid supercapacitors are available. In this context, supercapacitors, which are also sometimes referred to as ultracapacitors or electrochemical capacitors, offer remarkable power performance, good reversibility, extremely long cycle life [92]. (> 1000000 cycles), a simple working mode, and the ability to integrate into electronics. They also produce less thermochemical heat since the charge storage techniques that they use are so straightforward .Because of this, it has found widespread use in consumer electronics, memory backup systems, as well as in the power and energy management in industrial settings.

At this time, it is planned that it will be used in a variety of energy storage systems, including huge industrial machinery, electric cars, and portable electronic gadgets.

Particularly in the case of electric cars, it is anticipated that supercapacitors would have a larger energy storage capacity and power density, as well as ultra-superior characteristics such as the ability to resist lengthy cycles and have simple charge-discharge cycles. In order to ensure that these requirements are satisfied, it is essential that not just one, but all of the parameters be created simultaneously. For example, it is necessary to improve the properties of the collector material that is used as electrode material. This includes increasing the energy density of the material by making it porous and having a larger surface area. Concurrently, it is necessary to use a dielectric material that can withstand long cycles and is able to be charged and discharged quickly by simultaneously performing faradic reactions on this dielectric. According to the published research, in addition to the conventional components that are being built for this purpose, several next generation components are also being developed. The most crucial thing to anticipate from these components is that they will have a significant amount of surface area and a high level of conductivity. When compared to other types of metal oxides, the spinel-structured metal oxides have a better electrical conductivity than the other types of metal oxides. In most cases, the chemical composition of a spinel is written as AB_2O_4. Here, A symbolizes a divalent metal ion (M^{2+}), while B signifies a trivalent metal ion (M^{3+}). At a typical spinel structure, the ions A and B take up residence in tetrahedral sites and octahedral sites, respectively. Spinel ferrites, also known as MFe_2O_4 (where M = Mn, Co, Ni, Zn, Cu, etc.), are intriguing materials because of their remarkable magnetic, electrical, and optical characteristics, as well as the fact that they may display a variety of redox states and maintain their electrochemical stability [93]. $ZnFe_2O_4$ and Co_3O_4 electrodes are recognized for their non-toxic structure, large surface area, high specific capacitance, normal spinel structure, widely accessible metal salts, cheap cost, and environmental harmlessness [94]. In addition, these electrodes fall under the MFe_2O_4 and metal oxide categories [95]. In addition, both $ZnFe_2O_4$ and Co_3O_4 have large theoretical capacities, with the former having 2600 F/g and the latter having 3560 F/g [96]. Having large potential range ferrites ($ZnFe_2O_4$) is also so promising component in terms of energy storage density [97].

PART 4

LITERATURE REVIEW

4.1. CHALCOYRITE LEACHING

Carnie and Leao carried out a study by thinking that Cu concentration could be increased by removing passivation layer by NaCl [98]. For this purpose, they performed the extraction by 5.5 μm particle size chalcopyrite at 95 °C together with ferric chloride and sodium chloride. According to the result, they determined the Cu concentration as 95% with NaCl and without 45%. They also thought that the surface area and porosity of chalcopyrite increased with the addition of NaCl and contributed to the extraction.

Liddicoat and Dreisinger. investigated two methods of chloride leaching of chalcopyrite [99]. For this purpose two new treatment flowsheets were developed, combining chloride leaching of copper from chalcopyrite and solvent extraction . Both treatment schemes were designed similarly with two-stage countercurrent leaching but differ in iron deposition. Optimal leach extraction conditions were determined by varying the grind size, temperature and residence time for both scenarios. Experiments performed for the hematite model resulted in copper extractions of N95% while the goethite model only extracted 89% of the copper under comparable optimal conditions.

Bevilaqua et al. experimented the effect of sodium chloride on the bioleaching of a chalcopyrite concentrate in shake flasks and shake tank bioreactors [100]. The chloride is approved for leaching at high temperatures. Sodium chloride at a concentration of 100 mM did not affect the chemical leaching of copper from chalcopyrite at mesophilic temperature. Over time, the appearance of bacteria, ferrous iron and sodium chloride improved the leaching and the appearance of solid residues as shown by the analyses (X-ray reaction; XRD; EIS).

Ghorbany et al . studied the dissolution of copper in chalcopyrite by copper and chloride ion concentrations [101]. The procedure was carried out at a constant temperature of 60 degrees Celsius with the concentration of copper and chloride ions varying at two different pH values (1 and 2). They found that in the presence of high concentration of CU^{2+} and mainly in the presence of chloride, it gives a high extraction of copper. They also stated, from all the tests performed, that the best copper extractions were at pH 1 and not at pH 2.

Zhang et al . improved the leaching of chalcopyrite in sulfuric acid solution at mesophilic temperature using chloride and ammonium [102]. The study involved the synergistic catalytic effect of chloride Cl and ammonium (NH^{4+}). Similar promoting effects on chalcopyrite leaching were observed with chloride salts containing different cations (Na^{+}, K^{+}, Ca^{2+}, Mg^{2+}), revealing the crucial role of Cl, which acted as a complexing agent to stabilize Cu^{2+}/Cu^{+} while driving the leaching reaction. It was also shown that Cl and NH^{4+} have a synergistic activity, which may speed up the lixiviation of chalcopyrite in H_2SO_4 solution without adding any more Cl or NH^{4+} in an H_2SO_4 solution with no added oxygen.

Bogdanović et al. studied chalcopyrite concentrate leaching in hydrochloric acid with triple oxidizer hydrogen peroxide [103]. Metal extraction was studied in relation to the following leaching variables: stirring speed, solid-liquid ratio, temperature, and HCl and H_2O_2 concentrations There was a maximum final copper extraction of 33% after 80 minutes of reaction with 3.0 mol/L H_2O_2 in 0.5 mol/L HCl at room temperature in these processes. Additionally, they discovered that copper extraction was highest in the first 60 minutes of the process, and then dropped down significantly after that owing to the quick catalytic destruction of hydrogen peroxide.

For the purpose of extracting copper from chalcopyrite and removing iron as hematite, Jianming et al utilized ferric and cupric chloride in a nitrogen environment at 97 °C [104]. After 3-4 weeks of leaching, they found that copper extraction was 99% and iron extraction was 90% within these conditions. They found that by decreasing the chalcopyrite particle size from 26 μm to 15, copper and iron extractions went up by 0.2% and 2%, respectively. Copper ions are said to minimize the available elemental

sulfur to create copper sulfide and limit the copper extraction process when the Cu(II)+Fe(III) concentration in the leaching solution falls below 0.04 M.

The kinetics and mechanism of chalcopyrite's dissolution have been the subject of several scientific investigations. As an alternative, Solis et al. proposed that organic solvents added to the extraction solution would be sufficient to remove the passivation layer [105]. So as to achieve this goal, chalcopyrite was leached in an acid solution containing various oxidants (H_2O_2, $CuSO_4$, and O_3) with alcohols such 2-propanol and methanol at various temperatures. Results showed that copper dissolving in 2-propanol and hydrogen peroxide at 40 degrees Celsius required an activation energy of 42 kJ mol-1, a value they said is compatible with the decreasing core concept. The decomposition of peroxide at temperatures over 40 °C, however, reduced its efficacy. They found that the production of the banned (Cu_2S_2-$6Cu_2S$) was made possible due to the presence of methanol, which is essential for achieving high copper extraction.

Tong et al. claimed that passivation on the surface of the chalcopyrite was a significant issue and that it might be solved by bioleaching [106]. In this specific instance, it was said that the passivation layer was degraded by the addition of particles, resulting in an increase in the amount of copper extracted from 50% to 89.9%. SEM and XRD chalcopyrite surface examination validated these finding.

Deniz et al. explored chalcopyrite leaching using NaCl as an oxidant in ammonium persulfate-APS. They reported that the efficiency of metal extraction improved with increasing concentrations of NaCl, APS, leaching temperature (up to 333 K), and L/S ratio. Low metal extraction is caused by the creation of an elemental sulfur layer on the particle surface during oxidative leaching of sulfur minerals. They came to the conclusion that the sulfur layer may solve both the issue of poor solubility and the passivation effect that occurred when chloride ions were present the experimental findings showed 75% copper and 80% iron extraction efficiencies: APS 250 g/L, NaCl 150 g/L, 180 minutes, 333 K, 400 rpm, and L/S 250 mL/g.

4.2. ENERGY DEPOSITION PROCESS

Polat and Muwafaq synthesized $MgFe_2O_4$ (MFO) with g-C_3N_4 (g-CN) for increasing of electrochemical performance of MFO. The electrodes were produced directly on the surface of the nickel foam by using a hydrothermal manufacturing procedure. In order to provide a comprehensive description of the electrodes, XRD, FTIR, SEM, and TEM investigations were carried out. Electrochemically, CV, GCD, and EIS measurements were carried out at a variety of scanning speeds and current densities. According to the results, a g-CN-MFO electrode with a sponge-like structure was effectively synthesized on Ni-foams. It was determined that the areal capacitance (Ca) of g-CN-MFO was 600 mF/cm^2, which is 152% greater than that of MFO [107].

Polat and Muwafaq investigated the effect of graphene on magnesium iron oxide ($MgFe_2O_4$) in terms of electrochemical properties. The preparation of the electrode was carried out using a hydrothermal method, and it was done so directly on the surface of the nickel foam. X-ray diffractometry (XRD), Fourier transform infrared spectroscopy (FTIR), X-ray photoelectron spectroscopy (XPS), scanning electron microscopy (SEM), and transmission electron microscopy (TEM) were used in order to explore the crystallographic, Cyclic voltammetry (CV), galvanostatic charge-discharge (GCD), and electrochemical impedance spectrometry (EIS) were the methods that were used in order to carry out an analysis of its electrochemical properties. The results of the characterization show that $MgFe_2O_4$ was effectively synthesized using GNPs in a porous structure on a Ni foam surface. This was shown by the findings of the characterization [108].

S. Polat and Dana Faris synthesized CuFe2O4 crystals on a Ni foam surface (with g-C_3N_4, GNPs and individually) with the aim of utilizing it as a component in supercapacitors. They employed the hydrothermal method. They successfully created these materials, as proven by the results of their XRD, FTR and XPS analyses, which displayed a nanosponge-like geometry. From their experiments, they discovered the highest capacitance of 989 mF/cm^2 at 2mA (when all three elements were present), and the stability of the electrode after 1500 cycles was 70% at 16 mA. Additionally, the energy and power densities were 27.8 mWh/cm^2 and 300 mWh/cm^2 respectively.

They noted that the carbon-based component improved the specific capacitance (Cs) value by reducing the charge transfer and diffusion resistances of the electrodes. In conclusion, they stated that the high Cs value and low stability make this electrode suitable only for low cycle applications [109].

PART 5

EXPERIMENTAL PROCEDURE

5.1. MATERIALS

As shown in figure 5.1., the chalcopyrite particles employed in this thesis came from the Kastamonu Hanonü area and had a particle size of 1-6 m. After drying at 60 °C, it was immediately kept in plastic containers with caps. Copper and iron were extracted from chalcopyrite using deionized water, Nitric acid (HNO_3) Hydrochloric acid (HCL), Sulfuric acid H_2SO_4, and urea (CH_4N_2O) in the tests. The conductivity of the deionized water is 18.25 Mohm and it was produced by four resinous MARGEM water filters. Rokkim supplied HNO_3 HCL H_2SO_4 , while the Aromel chemical business supplied urea. On the surface of the nickel foam acquired from the Nanography firm, nanoparticle manufacturing operations were conducted after extraction. The nanoparticle synthesis was conducted in an autoclave walled with Teflon and stainless steel. This research was conducted at the Karabuk University Materials Research and Development Center using all laboratory equipment and analytical instruments (MARGEM).

Figure 5.1. The image of chalcopyrite used in the experiments .

5.2. PREPARATION OF LEACH SOLUTIONS

The procedures of making solutions with varying characteristics are broken down and discussed in order to facilitate the extraction of copper (Cu) and iron (Fe) elements from chalcopyrite. In order to accomplish this goal, first, 250 ml capacity of beaker was taken for making extraction process. In the first time, 3-gram chalcopyrite powder was weight than added into baker. After that the baker was placed on the magnetic stirrer and it was stirred at about 30 minutes. Than it was taken and filtrated firstly by Watman filter paper as seen in figure 5.2 than centrifuged at 3000 rpm by 15 minutes. Except for that, another same baker was used for acid incudes extractions. For this, 0.5 ml acid, 50 ml deionized water and 3-gram chalcopyrite was added into the baker and the same extraction process was applied by different concentration acids. As acid, hydrochloride, sulfuric and nitric acid was used at about 0, 10, 20, 30 and 40 ppm concentrations.

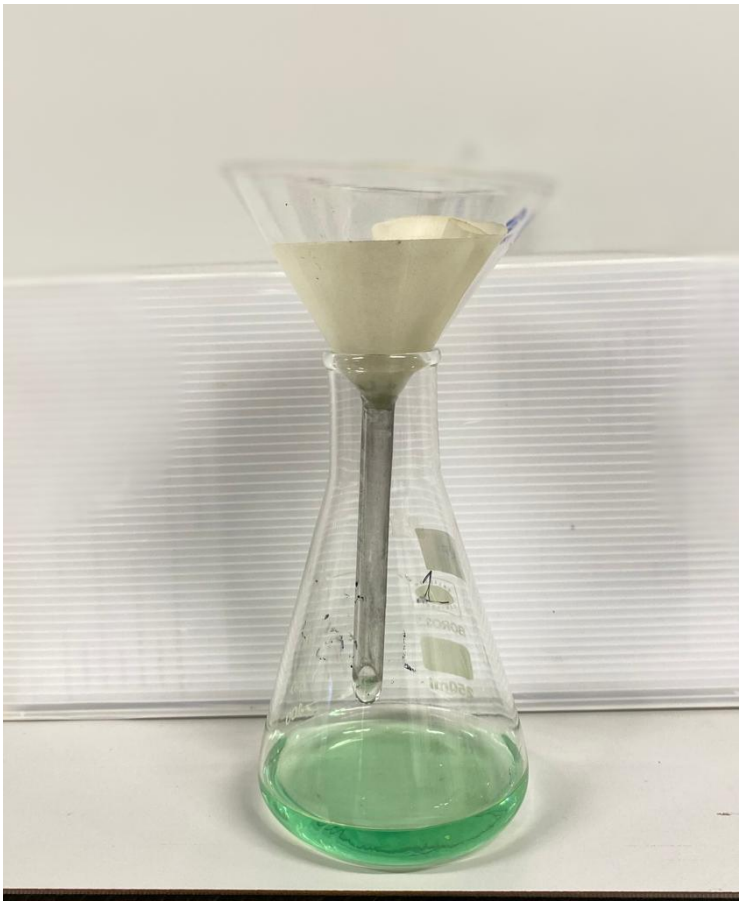

Figure 5.2. Filtration procedure.

Atomic absorption spectrometers with the model number THERMO SCIENTIFIC ICE 3400 were used to measure the amounts of copper (Cu) and iron (Fe) in the solutions (stock solutions) produced following extraction (AAS). A dilution into stock solutions was the first step in the beginning of this procedure. Because the Cu and Fe contents in the stock solutions are higher than the AAS measurement limit, this dilution is being done for the goal of reducing those levels. In order to carry out this procedure, the first thing that was done was to take 500 microliters of stock solutions and combine them with 50 ml of deionized water to create 5 M measurement solutions. Dilute solutions were the name given to these examples. On the other hand, additional solutions of 1 ppm, 3 ppm, and 5 ppm were generated independently from 1000 ppm Cu and Fe standard solutions using the same dilution technique. These other solutions, which were referred to as calibration solutions, were prepared for the measurement. The flame measuring component of the apparatus, together with copper and iron cathode tubes, was used to carry out the measurements. After the activation of the Cu tube, which took around 15 minutes, the next step was to wait for it to reach a stable state. After that, a technique was developed, with the first three measurements being made up of calibration solutions and the subsequent measurements being made up of samples of diluted measurement. This approach was used to begin the measurements, and the first thing that was done was to measure the concentrations of standard solutions with strengths of 1, 3, and 5 parts per million. It was stated that it should give 0.4 absorbance at 1 ppm concentration according to the results in the flame measurement standard of the Cu element in the software, and the measurement results of the standard solutions were obtained in this direction. This was also the case with the flame measurement standard of the Ni element. The procedure was completed by determining the concentration of the diluted sample measurements. The same method was used while working with Fe. Based on the findings presented here, the concentrations of copper and iron in the stock solutions were determined using a straightforward ratio and expressed in ppm units. Following extraction, each of the stock solutions were subjected to the same method of measurement. The following are the solutions that were created by the AAS apparatus that was utilized for this purpose. These preparations and measurements are shown in figure 5.3 and Fig. 5.4.

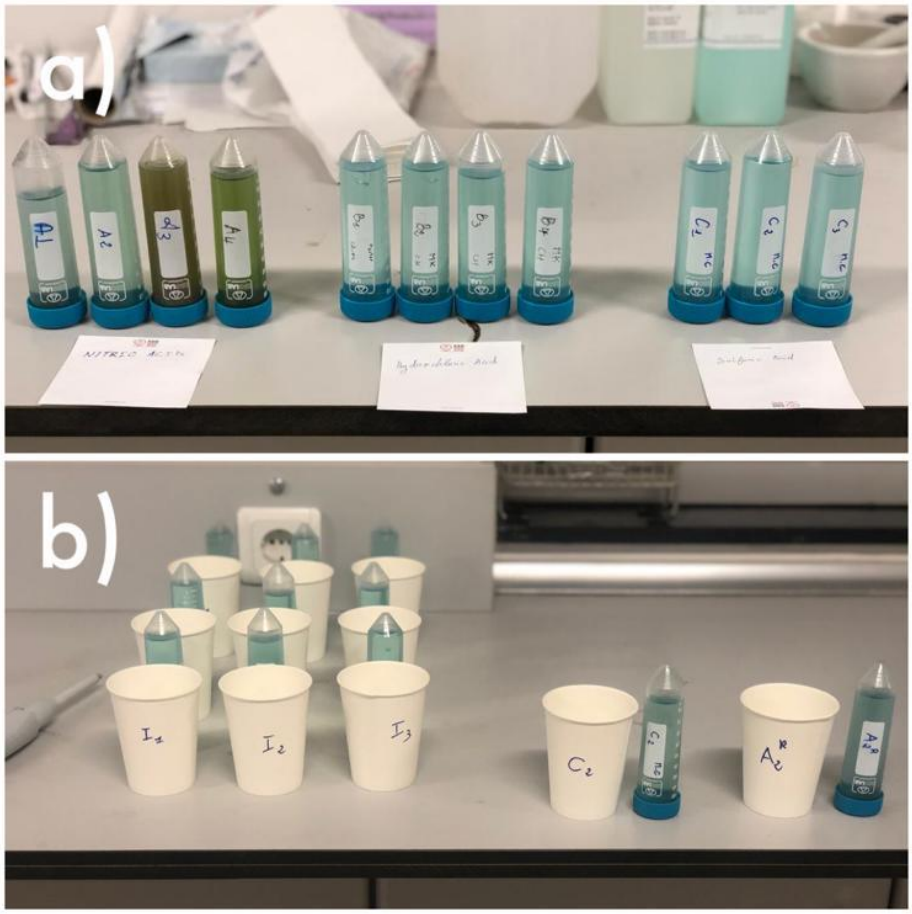

Figure 5.3. a) Post-extraction solutions and b) diluted solutions for AAS measurement

Figure 5.4. Atomic absorption spectroscopy (AAS).

For the goal of the thesis investigations, it is also extremely necessary to make use of copper and iron in solutions following the extraction of minerals rich in copper and iron, such as chalcopyrite, since this will further the research. For this reason, although though the aforementioned elements are often attempted to be gotten in their metallic form, it is very necessary in particular areas to get them in their metal oxide form. This is because of the purpose for which they are being obtained. When it comes to the efficiency of energy storage, nanosized metal oxide production on the surface of a metal collector substrate is very significant, and this is especially true for supercapacitors. In light of this, the purpose of this section of the research is to attempt to produce Cu-Fe-based metal oxide nanoparticles from the solution that has the highest concentration of Cu and Fe extraction from chalcopyrite as seen in dried version in figure 5.6. This is in accordance with the information that can be found in the relevant published works. The nanoparticle supercapacitors that are going to be produced at this stage are going to be used for the purpose of storing electrical energy at the anode electrode. Because of this need, the synthesis must take place on a conductive substrate. Because of its very high surface area, nickel foam is often utilized as a conductive substrate in supercapacitors. This element is among the most widely used. On nickel foam, the purpose of this investigation is to attempt to create metal oxide nanoparticles, the composition of which is anticipated to include Cu and Fe. The hydrothermal technique is one of the most appropriate ways that may offer nanoparticle synthesis in a liquid environment and on a substrate. It is also one of the most widely used methods. Before beginning production using this approach, the solution that had the greatest concentration after the previous step was identified first. This was done so that the production could begin. After that, ten milliliters of this solution were transferred into an autoclave made of stainless steel and Teflon that had a capacity of forty milliliters. This autoclave also received two pieces of nickel foam that had been cut to dimensions of one by three at the same time as seen in figure 5.7. After that, first the roof of the Teflon liner was securely closed, and then the cover of the autoclave made of stainless steel was secured. The same procedures were carried out in the other two autoclaves, bringing the total number of autoclaves that were used in the manufacturing to three.

After that, the autoclaves were put into the oven as seen in figure 5.5 and heated to a temperature of 150 °C at 10 °C/min. They remained at that temperature for a period of six hours. Following the completion of this procedure, the autoclaves were taken out of the oven and allowed to return to their normal temperature. After that, the caps were opened, and the nickel foams were removed before being rinsed in deionized water to eliminate any residues that may have been on them. Then after, it was dried at a temperature of sixty degrees Celsius for twenty-four hours and then subjected to dryer. In addition, since the solutions in the autoclave also include particles of the produced product and may be used in the procedures of characterization, they were transferred into glass tubes and centrifuged at 3500 revolutions per minute for 10 minutes. Then, the liquid that had been left over was emptied away, and the particles that had been left behind as precipitate were dried in the oven for 24 hours. As a result, the operations involved in the creation of nickel foam were carried out as seen in figure 5.8.

Figure 5.5. Protherm oven with high temperature.

Figure 5.6. Dryied solution before nanosynthesis

Figure 5.7. Teflons and autoclaves used in the hydrothermal process

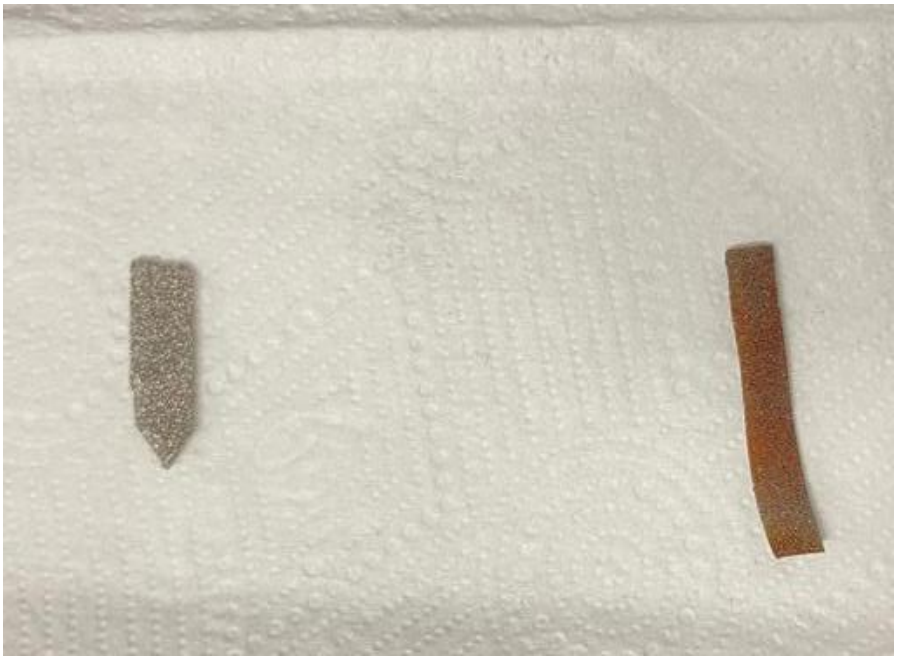

Figure 5.8. Macro view CFO coating with hydrothermal method

5.3. EXPERIMENTAL SYSTEM AND DEVICES

Crystallographic analysis using the Rigaku Ultima IV X-ray diffraction (XRD) device was the first step in the process of characterizing the products that were obtained after the metal oxide synthesis process on the nickel foam surface using the hydrothermal method. This was done so that the products could be properly classified. In these examinations, Cu-based Ka radiation with a wavelength of 0.1546 nanometers was used. The monochromator was maintained at 40 kilovolts and 40 milliamperes, and the 2 value was varied from 10-80 degrees. Then, in order to conduct an investigation into the chemical bonds that are present in these items, transmission mode Fourier transform infrared spectroscopy of the Bruker Alpha brand was used to conduct analyses between 400 and 4000 cm-1 in wave number, with a resolution of 2 cm-1 (FTIR). In addition, a Carl Zeiss ULTRA PLUS Scanning Electron Microscope was used in order to investigate the microstructure as well as the morphological pictures of these component parts (SEM). Figure 5.9, Figure 5.10, and Figure 5.11 each provide a visual depiction of one of the devices that was used for this specific objective.

Figure 5.9. X-ray diffraction instrument (XRD).

Figure 5.10. Fourier transform infrared spectroscopy (FTIR).

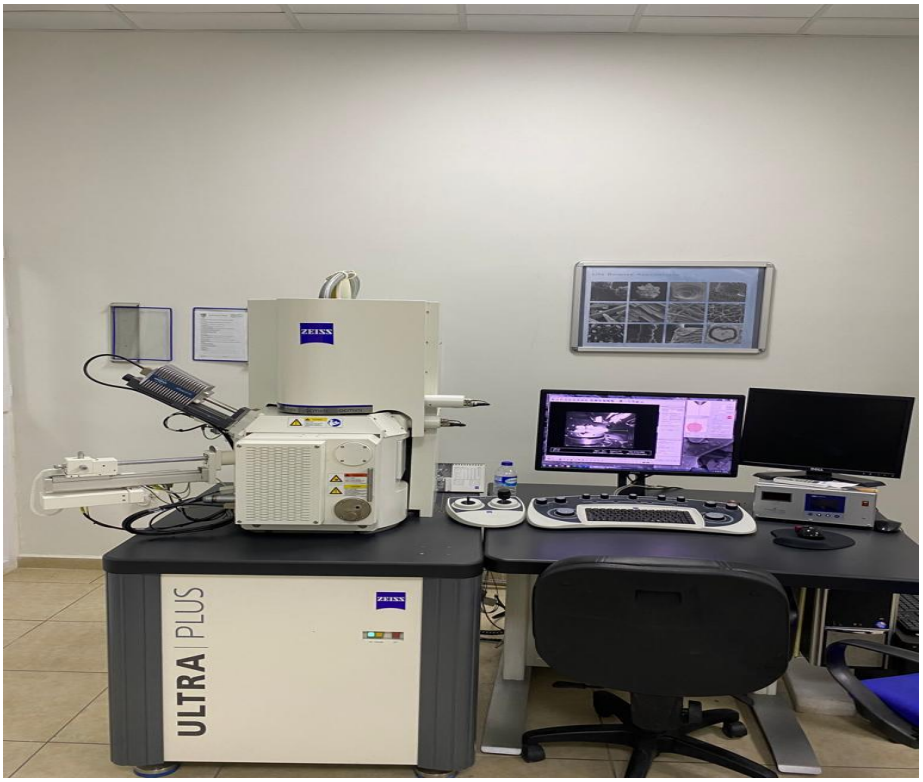

Figure 5.11. Scanning electron microscope (SEM).

5.4. ELECTROCHEMICAL MEASUREMENS

At normal temperature, the electrochemical performances of metal oxides that were formed directly on nickel foam surface by hydrothermal process from extraction solution were examined using a potentiometer device of the brand Parstat 4000. In these investigations, a testing equipment with three electrodes was used. As can be seen in Figure 5.12, graphite was employed as the counter electrode, Ag/AgCl was used as the reference electrode, and metal oxide doped nickel foam was used as the working electrode. The measurements were taken in a solution containing 6 M of KOH. Deionized water with a resistance of 18.25 Mohm was used in the preparation of this solution. In order to get the nickel foam as flat as possible before beginning the tests, a force of about 10 MPa was applied to it. The KOH solution was then transferred to a beaker, and the electrodes were submerged in the solution at this point. The working electrode, which consisted of nickel foam, was set such that it would be submerged in this solution to a depth of about 1 cm^2. Following the completion of this procedure, galvanostatic charge discharge measurements were carried out using the

Versa studio software program within the range of 1-6 mA. The discharge periods at each current density were calculated based on these results. After that, values for the particular areal capacitance, denoted by Ca, were determined by using the method found in Equation[107] .

$$Cs = \frac{I \times \Delta t}{\Delta V \times S} \tag{5.1}$$

In this formula, the value Ca represents the area capacitance in millifarads (mF), I represents the discharge current constant in milliamperes (mA), Δt represents the discharge time in seconds, V represents the potential window in volts, and S represents the surface area of the working electrode in square centimeters. In addition, the energy (E) and power (P) densities of the electrode were computed using Equations 5.2 and 5.3 according to the data that was acquired from this location.

$$\mathrm{E} = \frac{Cs \times V^2}{7.2} \tag{5.2}$$

$$\mathrm{P} = \frac{3600 \times E}{\Delta t} \tag{5.3}$$

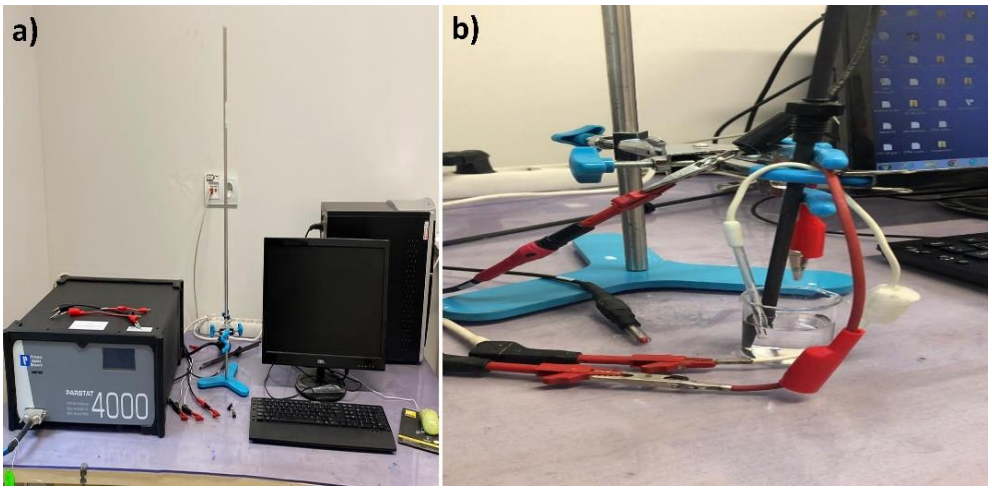

Figure 5.12. Electrochemical instruments a) potantiometer b) three electrodes cell

PART 6

EXPERIMENTAL RESULTS AND DISCUSSION

6.1. EXTRACTION RESULTS

The first part of this thesis consists of extracting copper and iron elements from chalcopyrite raw material. In this part, hydrochloric acid (HCl), sulfuric acid (H_2SO_4), and nitric acid (HNO_3) were used for extraction. The concentrations of these acids were adjusted as 0 ppm, 10 ppm, 20 ppm, 30 ppm, and 40 ppm. Other details are described in the experimental procedure section. The obtained results are given in Figures 6.1 and 6.2. According to these results, it was measured that copper and iron were at a concentration of 230 ppm in the extraction process with pure water without adding any acid. When 10 ppm HCl was added, this value reached 330 ppm for copper and 350 ppm for iron. In the case of adding 20, 30, and 40 ppm of HCl, the copper concentration reached 400, 460, and 466 ppm, respectively, while the iron concentration reached 375, 400, and 427 ppm. In the case of adding 10, 20, 30, and 40 ppm of H_2SO_4, the copper concentration was approximately 393, 457, 431, and 422 ppm, respectively, while the iron concentration was measured as 350, 410, 388, and 395 ppm. The same measurements were observed as approximately 422, 466, 492, and 481 ppm for copper and 385, 420, 446, and 433 ppm for iron with the addition of 10, 20, 30, and 40 ppm HNO_3. According to these results, it was observed that the highest concentration for both copper and iron was obtained with the addition of HNO_3. This increase was calculated to be 113% for copper and approximately 94% for iron in terms of quantity compared to the experiments with pure water. After HNO_3, the highest increase occurred with HCl and H_2SO_4 acids, respectively. The increase rates of copper and iron with HCl were approximately 102% and 85%, respectively, and approximately 98% and 78% with the addition of H_2SO_4. A similar study was carried out in Mariam’s master's thesis [17]. In her study, NaCl, MgCl, and urea additives increased the extraction. According to the results of her thesis, she obtained copper

extraction with an additional high addition of around 400 ppm NaCl, while iron extraction was obtained with approximately 370 ppm of MgCl + urea additions. It is clearly evident that the extractions obtained with acid additions are higher compared to these. These results are in agreement with many other studies in the literature.

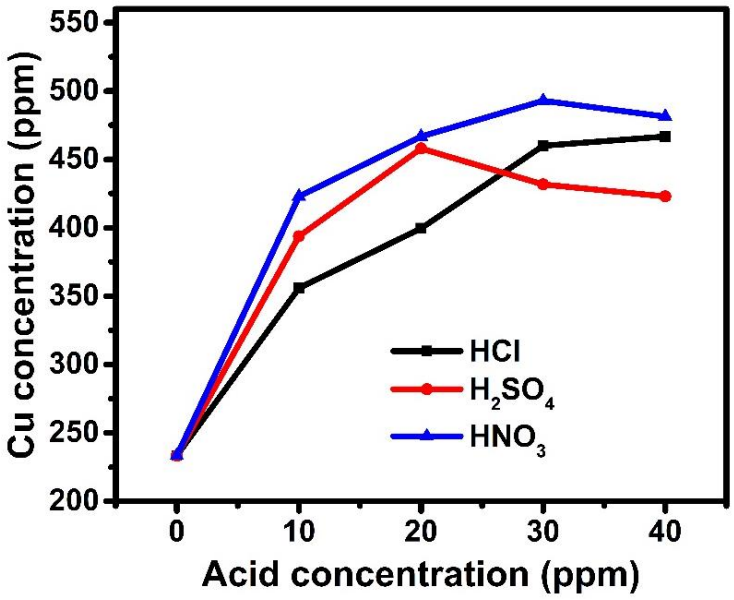

Figure 6.1. Copper extraction results in different acid concentrations .

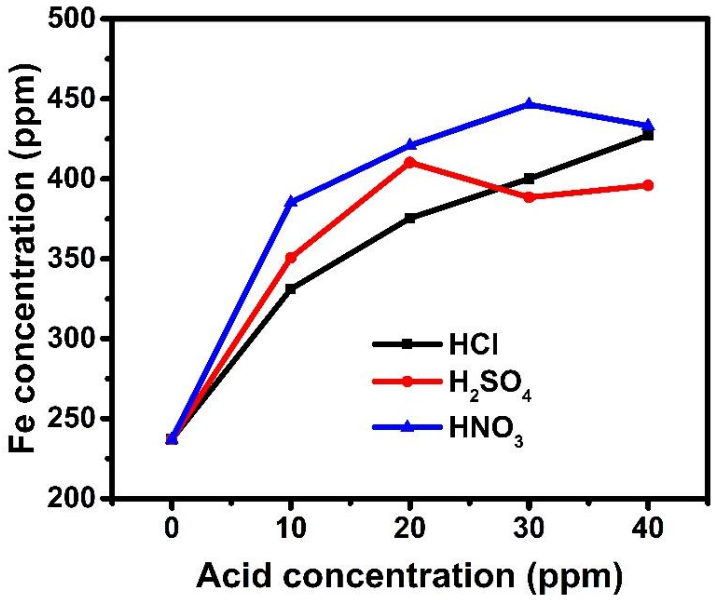

Figure 6.2. Iron extraction results in different acid concentrations .

6.2. MATERIAL CHARACTERIZATION RESULTS

The second part of this study is to characterization of synthesized metal oxides for usage as electrode materials in supercapacitors. The solution derived from the extraction procedure in the first section was applied for this purpose. Nitric acid solution, which is the richest in copper and iron and doesn't generate secondary reactions, was selected for this. After this solution was extracted, it was dried at 100 °C to produce powdered nitrate salts that contained iron and copper. To begin with, these powders were characterized using XRD analysis. The findings of this analysis are shown in figure 6.3. The results of chalcopyrite as a raw material and electrode material as a finished good are also shown in this graph. These findings indicate that the peaks found in the XRD graph of the raw material at 2θ values of roughly 30°, 49°, and 57°, respectively, derive from the (204), (331), and (511) planes of the chalcopyrite [110]. As the literature results confirm this, we can say that the material used as raw material is chalcopyrite. On the other hand, the XRD result of the nitrate salt drawn in red is also given in this graph. According to this result, the 2θ value is due to the (202), (400) and (204) planes of the copper nitrate, respectively, of the peaks observed at 18°, 24° and 29° [111]. In addition, the peaks observed at approximately 22°, 36° and 39° appear to originate from the (012), (110) and (113) planes of iron nitrate, respectively [112]. Apart from these, the XRD analysis of the product synthesized by the hydrothermal method is also given in blue. It can be said that the peaks observed at approximately 26° and 35° in this graph are due to the (112) and (312) planes, respectively, of the urea compound used during the synthesis [113]. In addition, the peaks observed in approximately 35°, 39°, 42°, 45°, 56°, 61° and 64° are copper ferrite (311), (222), (400), (331), (511), (440) and (300) planes. All of these peaks are in good agreement with the literature. At the same time, interatomic bond characterizations of these products were made by FTIR analysis, and the results were examined. Analysis results are given in Figure 6.4. According to these results, the low intensity peak observed at approximately 410-470 cm^{-1} is probably due to S-S bonds in Cu-Fe-S system [114]. These are probably also caused by sulfur bonds in the CuS and FeS_2 composition. On the other hand, vibration peaks for Cu-O and Fe-O bonds were also observed at wave number approximately 456 and 598 cm^{-1}, respectively [115]. Other carbon bonds are probably from urea and impurities.

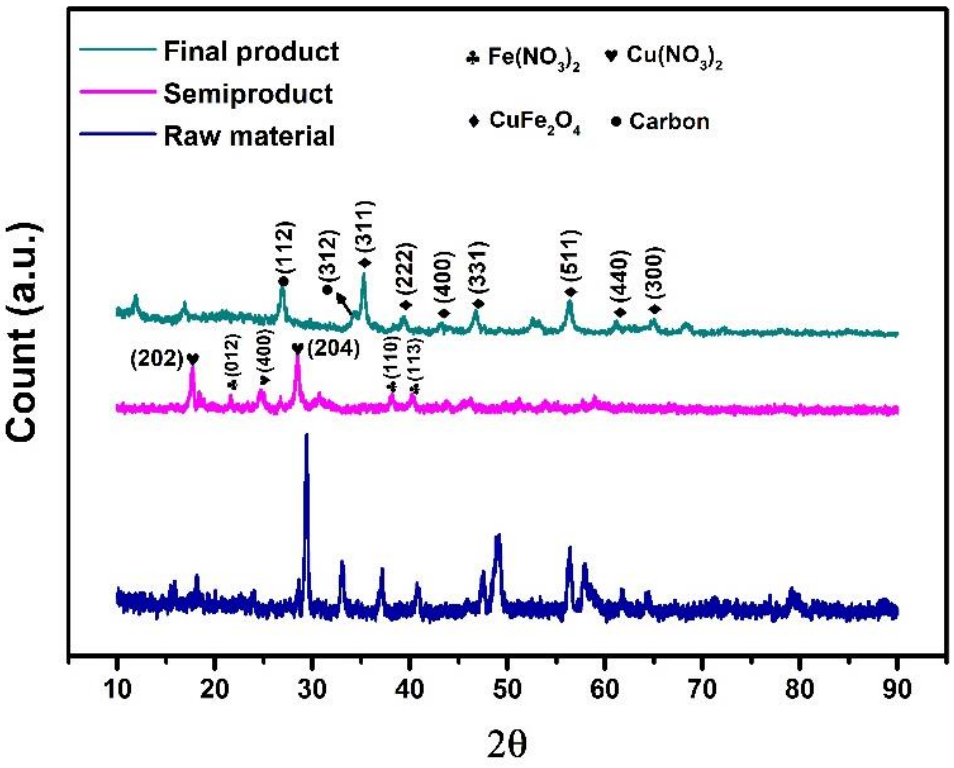

Figure 6.3. Xray defraction (XRD) analyses of materials

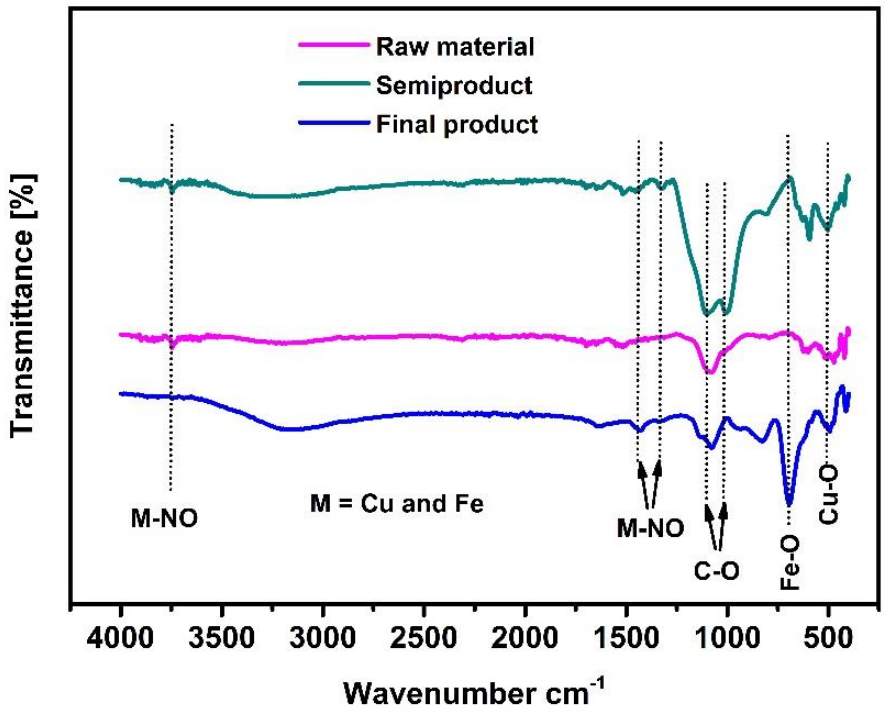

Figure 6.4. Fourrier Transform infrared (FTIR) analyses of materials

In this study, it was aimed to synthesize copper and iron-based metal oxides as electrodes from the acid extraction solution of chalcopyrite. Nickel foam was used as the current collector electrode. The synthesis process was carried out by hydrothermal method. Detailed information about the synthesis is given in the procedure section. In this section, there is an electron microscope examination and imaging of nickel foam before and after synthesis. These images are given in Figure 6.5 Figure 6.5a shows the surface of nickel foam before synthesis. It is observed that the surface is quite smooth and there are no joints here. In Figure 6.5b, there is the image of the surface after the synthesis, which reveals very homogeneous formations. High magnification observation was made to observe the geometric structure of these formations, which are given in Figure 6.5c and d. In these images, it can be said that the structures formed on the surface of Ni foam are rose, flower or cauliflower patterns. Many similar structures have emerged in the literature. These structures are said to be 2D and have a fairly large surface area. When the wall thickness was measured, it was found to be 25-50 nm on average, confirming its 2D structure. In this context, it is stated in the literature that these formations will provide a very high energy storage capacity by attracting more ions.

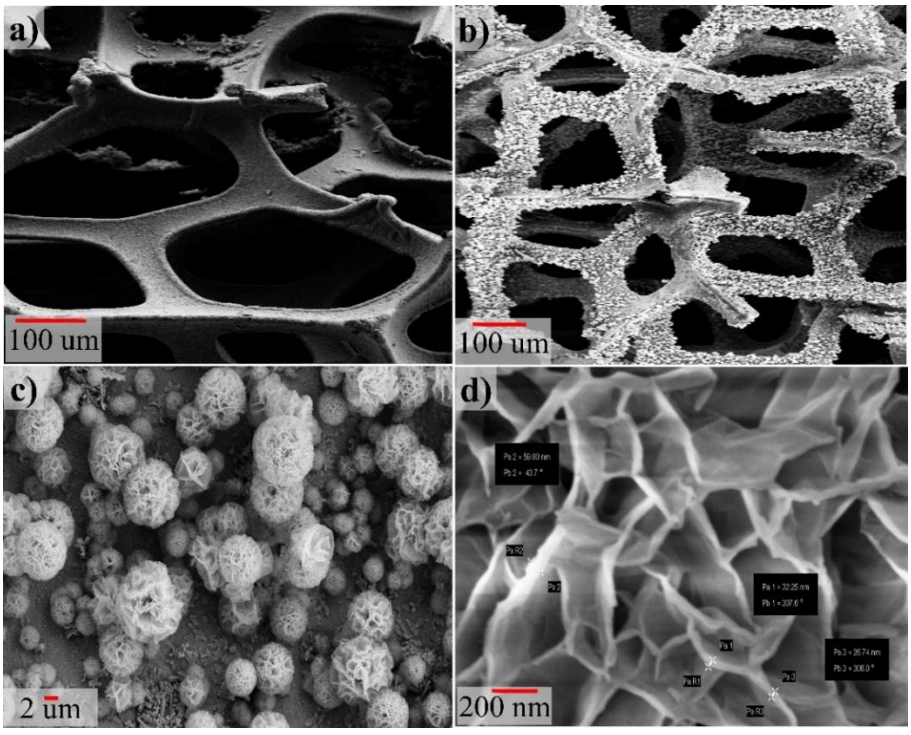

Figure 6.5. Scanning electron microscope images of a) pure Ni foam, b) metal oxide synthesized Ni foam, c and d) high magnification of metal oxides.

For the further characterization of these structures, general observation and high-resolution examination were made with a transmission electron microscope. These results are given in figure 6.6. In the visuals given in figure 6.6.a, strip structures were also observed apart from the plate structure in the SEM images. These are probably thin rod-like structures that cannot be seen in SEM. In figure 6.6.b and especially c, there are high resolution images. In these images, it can be seen up to atomic arrays. These arrays represent a plane. With Image J, the interplanetary distance in this figure 20c was measured to be 0.45 nm, which is probably due to the (200) plane of the $CuFe_2O_4$ metal oxide. This plane was also observed in the XRD results. These results show that 2D flower and rose-like $CuFe_2O_4$ crystals with a wall thickness of approximately 25-50 nm occur on the surface of nickel foam. It has been stated in the literature that similar results occur with different crystal types and that these structures provide significant advantages in terms of energy storage with their large surface area. For this reason, it can be said that successful results can be obtained in terms of quality from the results so far.

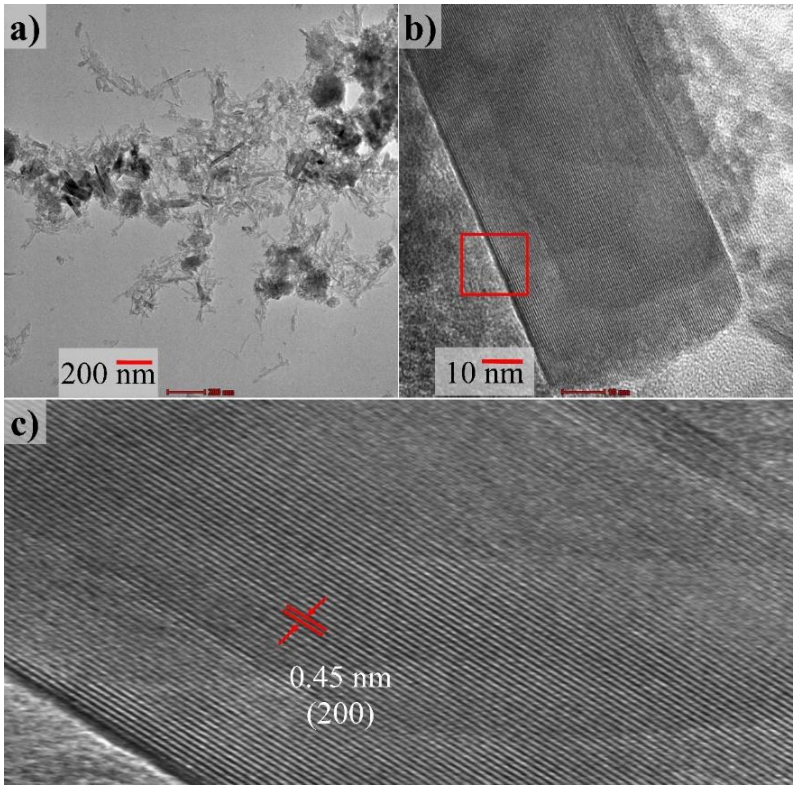

Figure 6.6. Transmission electron microscope a) general images, b and c) high resulotion images of synthesized metal oxide

6.3. ELECTROCHEMICAL RESULTS

To investigate the electrochemical performance of the electrodes produced by the hydrothermal method, cyclic voltammetry (CV) measurements were first performed at various scanning speeds. Figure 6.7 depicts the obtained results graphically. According to these results, positive peaks were observed in the cathodic region in the range of 0.25-0.30 V, whereas negative peaks were observed in the anodic region around 0.15 V and 0.065 V. Considering that the electrode material consists of Cu and Fe components, these peaks are thought to originate from Cu I-II and Fe II-III oxidation/reduction reactions. Furthermore, the presence of these peaks in both the anodic and cathodic regions implies that the surface reduction and oxidation events are reversible. The steady growth of these peak intensities in the anodic and cathodic areas as the scanning speed increases, on the other hand, is both an indication of reversible reactions and an indication that this electrode has a diffusion-controlled charging mechanism. All of these findings are already supported by research on Cu and Fe-containing electrodes.

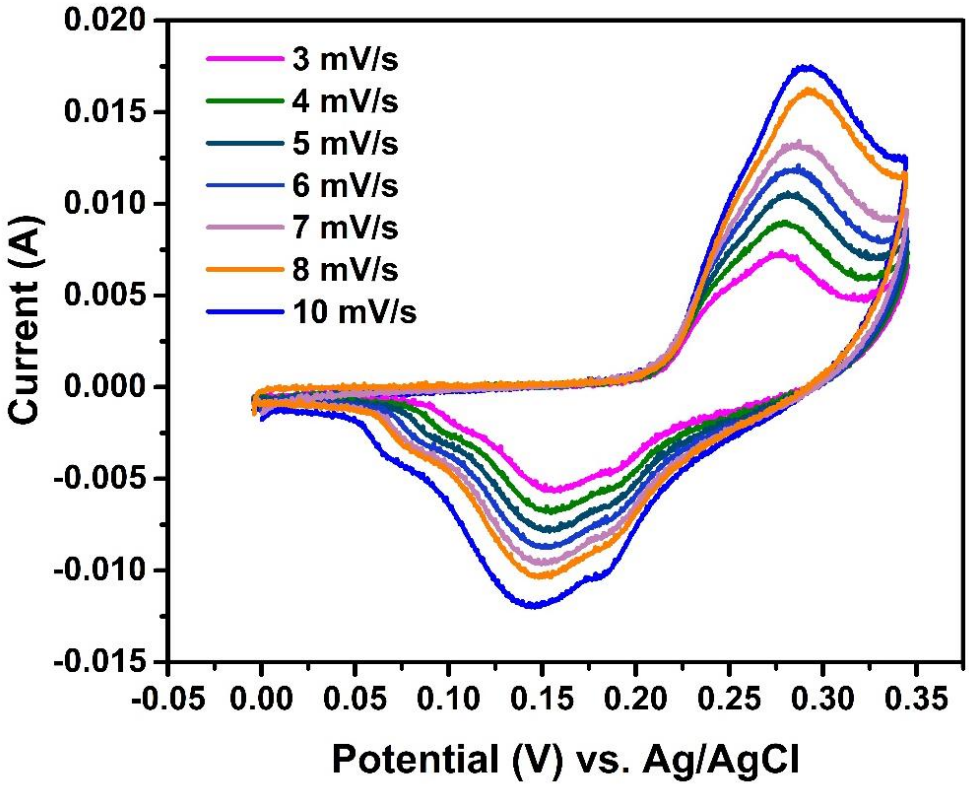

Figure 6.7. CV measurement results of the electrode at different scanning rate

Another electrochemical performance determination parameter is the galvanostatic charge-discharge measurement (GCD). With this measurement, the charge and discharge times of the electrode at different current densities are determined by chronoamperometry. Thus, the diffusion time and return of the ions in the solution to the electrode surface are determined. GCD measurement results made for this purpose are given in figure 6.8. According to these results, it can be said that a classical battery type charge-discharge curve occurred in all measurements. It is also understood that the discharge times gradually increase due to the decrease in current density. In this context, discharge times at current densities of 2 mA, 3 mA, 4 mA, 5 mA, 6 mA and 7 mA were determined to be 138 seconds, 84 seconds, 56 seconds, 40 seconds, 31 seconds and 25 seconds, respectively. These dates allow for the calculation of the electrode's specific capacitance, or its capacity to hold ions as a function of current density. Specific capacitance (Cs) values were determined using the formula presented in Chapter 5, equation 3.1, and the aforementioned nocturnal current densities were calculated to be 525 mF/s, 480 mF/s, 426 mF/s, 380 mF/s, 354 mF/s, and 333 mF/s, respectively. These results are given in the graph in figure 6.9 .

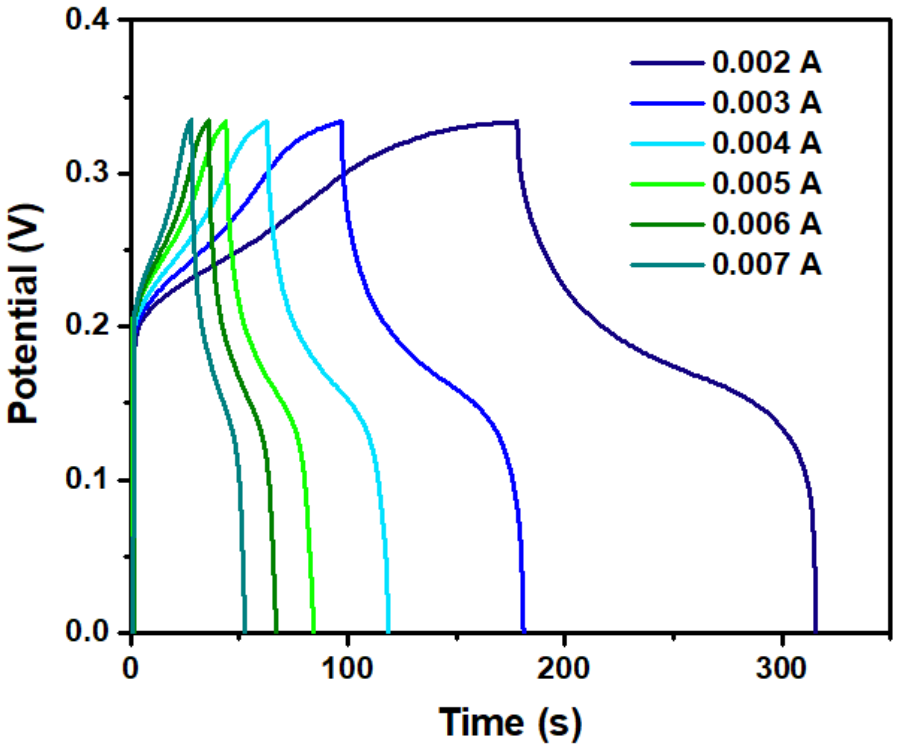

Figure 6.8. GCD measurement plots of the electrode at different current

As the current density increases, the decrease in the Cs value is directly related to the time-dependent variation of the ion-electrode interaction. At high current densities, ions accumulate on the electrode surface and quickly form a film layer, so they cannot move towards the inner parts of the electrode. However, at low current densities, ions gradually accumulate on the electrode surface, during which diffusion is ensured to the inner parts of the electrode. For this reason, at low current densities, more ions are attached to the electrode and the associated Cs value is quite high. This situation has been expressed in this direction in many studies carried out so far.

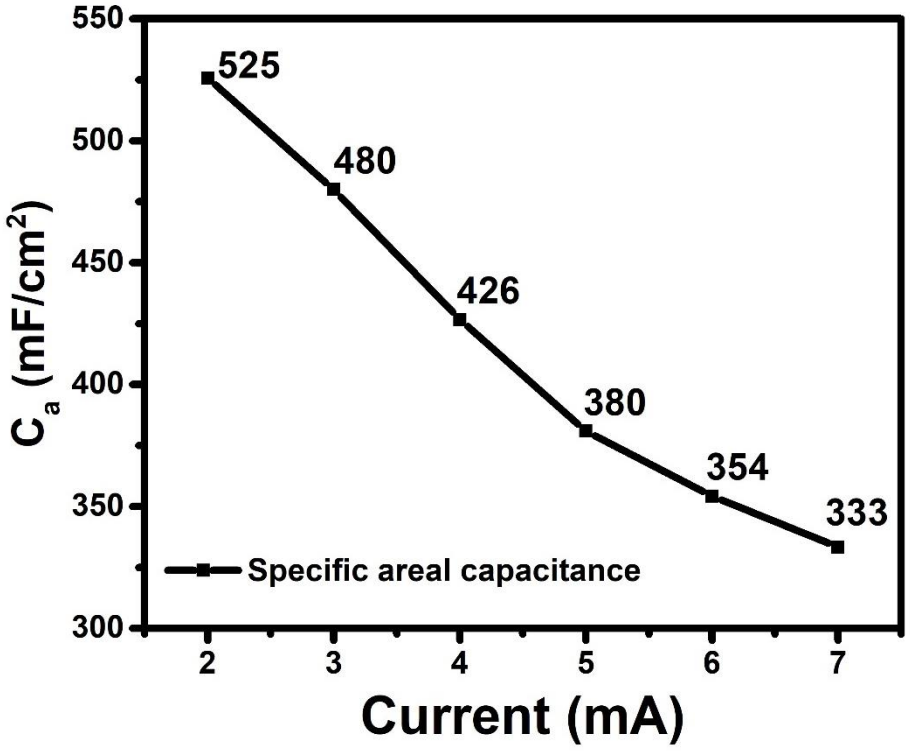

Figure 6.9. Specific capacitance calculation results vs. current plot of electrode

Apart from these, the electrode also has energy and power density values, which are very important in terms of evaluating the electrochemical performance. Formulas for both energy and power density calculations were given in equations 5.1 and 5.2 given under the heading of electrochemical characterization in Chapter 5. In the calculations made according to these formulas, the energy densities at current values of 2 mA, 3 mA, 4 mA, 5 mA, 6 mA and 7 mA are 8.9 mWh/cm^2, 8.1 mWh/cm^2, 7.25 mWh/cm^2, 6.48 mWh/cm^2, 6.02 mWh/cm^2 and 5.67 mWh/cm^2, while the power densities were calculated as 233 mW/cm^2, 350 mW/cm^2, 466 mW/cm^2, 583 mW/cm^2 and 816

mW/cm^2. These results are also given graphically in figure 6.10. According to these results, it is understood that the energy density decreases, and the power density increases due to the increase in current density. What is desirable in supercapacitors is that both energy and power density are high at the same time. However, these findings are directly related to the measured current value. For example, the 8.9 mWh/cm^2 energy density obtained at 2 mA is a high finding compared to those in the literature.

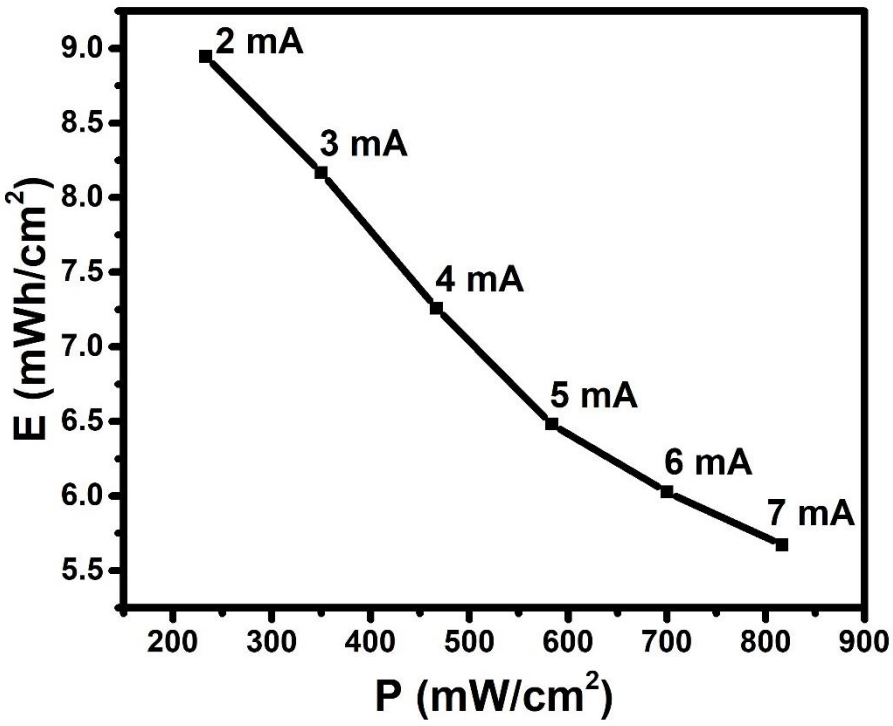

Figure 6.10. Energy (E) and power (P) density plot of electrode

PART 7

SUMMARY

This study mainly aims to produce electrodes from mineral for supercapacitors, a very common electrical energy storage tool today. First, the requirements of a supercapacitor in terms of charge storage mechanism have been determined. These are the large surface area of the electrode and its ability to give an oxidation/reduction reaction. While a large surface area can be achieved using nano-sized synthesis methods, redox reactions can be carried out with metal oxides. Considering these requirements, copper and iron-containing chalcopyrite was chosen as a mineral that can give a redox reaction. Firstly, leaching solutions of HCl, H_2SO_4, and HNO_3 acids at 0 ppm, 10 ppm, 20 ppm, 30 ppm, and 40 ppm concentrations were prepared for the hydrometallurgical extraction of copper and iron from this mineral. Then, 3 grams of chalcopyrite mineral was added to these solutions, mixed for 30 minutes at 360 rpm stirring speed, and then centrifuged to obtain extraction solutions. Elemental measurements were made with AAS to determine each solution's copper and iron concentrations, and the results were presented in graphics. The results were measured as 492 ppm and 446 ppm, respectively, with 30 ppm HNO_3 acid of the highest copper and iron concentrations. Later, this solution was used for metal oxide synthesis on nickel foam surface by hydrothermal method. After the synthesis process, the chemical head oil of the products was examined with FTIR, and the crystal structure of the products was examined with XRD. It was observed that $CuFe_2O_4$ metal oxide was formed in general, despite some impurities. The geometric and morphological structure of these formations were also examined by SEM and TEM examined, and results showed that crystals with a flower pattern of approximately 25-50 nm wall thickness were formed. It has also been found that the interplanetary distance in high-resolution imaging is compatible with the XRD results.

On the other hand, its electrochemical performance was measured by CV and GCD analysis. CV measurements showed that oxidation and reduction reactions occur reversibly in the anodic and cathodic regions. It is thought that these peaks are probably due to Cu-I-II and Fe-II-III transformations. In addition, it can be said that the electrode synthesized according to the CV graph has a battery-type battery cycle character. In the GCD measurements, the discharge times of the electrode at different current densities were measured, and the specific capacitance values were calculated. Accordingly, the highest specific capacitance value was calculated as 525 mF/cm2 at a current density of 2 mA/cm2. In addition, the energy and power densities of the electrode, depending on the discharge and specific capacitance value, were also calculated, and it was observed that they were approximately 8.9 mWh/cm^2 and 233 mW/cm^2, respectively. These values are quite high compared to pure $CuFe_2O_4$ metal oxide electrodes in the literature. As a result, this study aims to contribute to the literature by systematically examining these processes for producing an electrode from chalcopyrite. Examining the results obtained by comparing them with the data in the literature has enabled this aim to be realized.

REFERENCES

1. Wang, P., Li, N., Li, J., and Chen, W.-Q., "Chapter 3 - Metal-energy nexus in the global energy transition calls for cooperative actions", The Material Basis of Energy Transitions, ***Academic Press***, 27–47 (2020).

2. Baştürkcü, E., Şavran, C., Timur, S., and Yüce, A. ekrem, "Birincil ve İkincil Mineral Kaynaklarından Nadir Toprak Elementlerinin Fiziksel ve Fizikokimyasal Yöntemlerle Üretim Proseslerinin İncelenmesi", ***International Journal Of Pure And Applied Sciences***, 7 (2): 276–287 (2021).

3. Mohamed El Mamy, M., "COPPER FERRITE SYNTHESIS FROM CHALCOPYRITE AND INVESTIGATION OF ITS ELECTROCHEMICAL PROPERTIES", Thesis, (2022).

4. Scappettone, J., "Agitating a Copper Lyre; or, geolyricism for the age of digital reproduction", Geopoetics in Practice, ***Routledge***, 15 (2019).

5. Frenzel, M., Tolosana-Delgado, R., and Gutzmer, J., "Assessing the supply potential of high-tech metals – A general method", ***Resources Policy***, 46: 45–58 (2015).

6. Tezġ, Y. L., "ĠSTANBUL TEKNĠK ÜNĠVERSĠTESĠ FEN BĠLĠMLERĠ ENSTĠTÜSÜ", 72 (2005).

7. Şenol, Ç. and Kervan, N., "RbX (X= Sb, Te) bileşiklerinin manyetik özelliklerinin yoğunluk fonksiyonel teorisi ile incelenmesi", MasterThesis, ***Nevşehir Hacı Bektaş Veli Üniversitesi***, (2013).

8. Strezov, V., Zhou, X., and Evans, T. J., "Life cycle impact assessment of metal production industries in Australia", ***Scientific Reports***, 11 (1): 10116 (2021).

9. Bakır, A. A., Atik, R., and Özerinç, S., "Mechanical properties of thermoplastic parts produced by fused deposition modeling:a review", ***Rapid Prototyping Journal***, 27 (3): 537–561 (2021).

10. Tantawy, A. A. G., Tadros, M. A. R., Adly, A. A. M., Ismail, E. A. R., Ibrahim, F. A., Salah Eldin, N. M., Hussein, M. M., Alfeky, M. A., Ibrahim, S. M., Hashem, M. A., and Ebeid, F. S. E., "Endothelin-1 gene polymorphism (G8002A) and endothelial monocyte-activating polypeptide II: Role in

vascular dysfunction in pediatric patients with β-thalassemia major", ***Cytokine***, 161: 156048 (2023).

11. "What Is New in Iron Overload? | SpringerLink", **https://link.springer.com/article/10.1007/s00431-007-0604-y** (2022).

12. "Material and Energy Flows of the Iron and Steel Industry: Status Quo, Challenges and Perspectives - ScienceDirect", **https://www.sciencedirect.com/science/article/pii/S030626192030458X** (2022).

13. Bahar, N., "Copper Recovery from Roasted Chalcopyrite Concentrate by Using Hydrochloric Acid or Water Leaching Method", ***International Journal Of Pure And Applied Sciences***, 1 (1): 1–8 (2015).

14. "Recycling Rare-Earth-Metal Wastes by Pyrometallurgical Methods | SpringerLink", **https://link.springer.com/article/10.1007/s11015-015-0111-8** (2022).

15. "Structural Phase Transition in CuFe2O4 Spinel | SpringerLink", **https://link.springer.com/article/10.1134/S1063774513040044** (2022).

16. Velásquez Yévenes, L., "The kinetics of the dissolution of chalcopyrite in chloride media", Phd, ***Murdoch University***, (2009).

17. Mohamed El Mamy, M., "COPPER FERRITE SYNTHESIS FROM CHALCOPYRITE AND INVESTIGATION OF ITS ELECTROCHEMICAL PROPERTIES", Thesis, (2022).

18. Rebolledo, M., "Kinetic study of the dissolution of chalcopyrite in the presence of a catalyst under acidic sulfate medium", ***University of British Columbia***, (2017).

19. Zeng, W., Liu, Z., Amanze, C., Cheng, J., Liao, W., Wu, X., Qiu, G., Wang, Q., Wu, Z., Zou, L., and Shen, L., "In situ detection of Cu2+, Fe3+ and Fe2+ ionsat the microbe-mineral interface during bioleaching of chalcopyrite by moderate thermophiles", ***Minerals Engineering***, 191: 107936 (2023).

20. "The Reductive Leaching of Chalcopyrite by Chromium(II) Chloride for the Rapid and Complete Extraction of Copper - Vardner - 2023 - ChemistryOpen

- Wiley Online Library", **https://chemistry-europe.onlinelibrary.wiley.com/doi/full/10.1002/open.202200196** (2023).

21. Panda, S., Akcil, A., Pradhan, N., and Deveci, H., "Current scenario of chalcopyrite bioleaching: A review on the recent advances to its heap-leach technology", ***Bioresource Technology***, 196: 694–706 (2015).

22. He, S., Huang, Y., Wang, C., Wang, M., and Zhang, Y., "Enhanced selective hydrophobicity performance at solid-liquid interface during separation of chalcopyrite from galena with 5-methyl isobutylxanthate-1,3,4-oxadiazole-2-thione", ***Surfaces And Interfaces***, 36: 102509 (2023).

23. Chi, W. and Banerjee, S. K., "Comparison and integration of CuInGaSe and perovskite solar cells", ***Journal Of Energy Chemistry***, (2023).

24. Makuei, F. M. and Senanayake, G., "Extraction of tellurium from lead and copper bearing feed materials and interim metallurgical products – A short review", ***Minerals Engineering***, 115: 79–87 (2018).

25. Knight, R. D., Roberts, S., and Cooper, M. J., "Investigating monomineralic and polymineralic reactions during the oxidation of sulphide minerals in seawater: Implications for mining seafloor massive sulphide deposits", ***Applied Geochemistry***, 90: 63–74 (2018).

26. Sun, K., Chen, B., Deng, J., and Ma, X., "Source of copper in the giant Shimensi W-Cu-Mo polymetallic deposit, South China: Constraints from chalcopyrite geochemistry and oxygen fugacity of ore-related granites", ***Ore Geology Reviews***, 101: 919–935 (2018).

27. Perlatti, F., Otero, X. L., Macias, F., and Ferreira, T. O., "Geochemical speciation and dynamic of copper in tropical semi-arid soils exposed to metal-bearing mine wastes", ***Science Of The Total Environment***, 500–501: 91–102 (2014).

28. Anawar, H. M., "Sustainable rehabilitation of mining waste and acid mine drainage using geochemistry, mine type, mineralogy, texture, ore extraction and climate knowledge", ***Journal Of Environmental Management***, 158: 111–121 (2015).

29. Carrillo-Chávez, A., Salas-Megchún, E., Levresse, G., Muñoz-Torres, C., Pérez-Arvizu, O., and Gerke, T., "Geochemistry and mineralogy of mine-waste material from a “skarn-type” deposit in central Mexico: Modeling geochemical controls of metals in the surface environment", ***Journal Of Geochemical Exploration***, 144: 28–36 (2014).

30. "Moving Metals III: Possible Origins for Copper in Bronze Age Denmark Based on Lead Isotopes and Geochemistry - ScienceDirect", **https://www.sciencedirect.com/science/article/pii/S0305440318301237** (2022).

31. Georgoudis, A., Larsen, K. J., and Zhang, Y., "Azurite: An algebraic geometry based package for finding bases of loop integrals", ***Computer Physics Communications***, 221: 203–215 (2017).

32. Feng, Q., Zhao, W., and Wen, S., "Surface modification of malachite with ethanediamine and its effect on sulfidization flotation", ***Applied Surface Science***, 436: 823–831 (2018).

33. Chen, X., Peng, Y., and Bradshaw, D., "The separation of chalcopyrite and chalcocite from pyrite in cleaner flotation after regrinding", ***Minerals Engineering***, 58: 64–72 (2014).

34. Guélou, G., Powell, A. V., and Vaqueiro, P., "Ball milling as an effective route for the preparation of doped bornite: synthesis, stability and thermoelectric properties", ***Journal Of Materials Chemistry C***, 3 (40): 10624–10629 (2015).

35. Zuo, Q., Wu, D., Cao, J., Wang, Z., Wen, S., Huang, L., and Chen, H., "Corrosion activation by ammonium fluoride enhances the separation of chrysocolla and quartz by sulfidation flotation", ***Minerals Engineering***, 189: 107864 (2022).

36. Han, G., Wen, S., Wang, H., and Feng, Q., "Sulfidization regulation of cuprite by pre-oxidation using sodium hypochlorite as an oxidant", ***International Journal Of Mining Science And Technology***, 31 (6): 1117–1128 (2021).

37. "Identification and Characterization of Basic Copper Sulfates as Mineral Green Pigments in Andean Colonial Mural Paintings: Use of Temperature-controlled Stage for the Study of Thermal Induced Antlerite Degradation - Tomasini - 2021 - Journal of Raman Spectroscopy - Wiley Online Library", **https://analyticalsciencejournals.onlinelibrary.wiley.com/doi/full/10.1002/jrs.6218** (2022).

38. Toro, N., Pérez, K., Saldaña, M., Jeldres, R. I., Jeldres, M., and Cánovas, M., "Dissolution of pure chalcopyrite with manganese nodules and waste water", ***Journal Of Materials Research And Technology***, 9 (1): 798–805 (2020).

39. "Exsolution of Chalcopyrite from Bornite-Digenite Solid Solution: An Example of a Fluid-Driven Back-Replacement Reaction | SpringerLink", **https://link.springer.com/article/10.1007/s00126-018-0820-6** (2022).

40. "CuFeS2 as an Anode Material with an Enhanced Electrochemical Performance for Lithium-Ion Batteries Fabricated from Natural Ore Chalcopyrite | SpringerLink", **https://link.springer.com/article/10.1007/s10008-019-04284-8** (2022).

41. Sadhukhan, S., Sadhukhan, B., and Kanungo, S., "Pressure-driven tunable properties of the small-gap chalcopyrite topological quantum material ${\mathrm{ZnGeSb}}_{2}$: A first-principles study", ***Physical Review B***, 106 (12): 125112 (2022).

42. Nyembwe, K. J., Fosso-kankeu, E., Waanders, F., and Mkandawire, M., "PH-dependent leaching mechanism of carbonatitic chalcopyrite in ferric sulfate solution", ***Transactions Of Nonferrous Metals Society Of China***, 31 (7): 2139–2152 (2021).

43. Klauber, C., "A critical review of the surface chemistry of acidic ferric sulphate dissolution of chalcopyrite with regards to hindered dissolution", ***International Journal Of Mineral Processing***, 86 (1): 1–17 (2008).

44. Lundström, M., "Chalcopyrite Dissolution in Cupric Chloride Solutions", ***Teknillinen Korkeakoulu***, (2009).

45. Agrawal, A., Kumar, V., Pandey, B. D., and Sahu, K. K., "A comprehensive review on the hydro metallurgical process for the production of nickel and copper powders by hydrogen reduction", ***Materials Research Bulletin***, 41 (4): 879–892 (2006).

46. "Combining Sulfate Electrowinning with Chloride Leaching | SpringerLink", **https://link.springer.com/article/10.1007/BF03221106** (2022).

47. Lundström, M., Aromaa, J., Forsén, O., Hyvärinen, O., and Barker, M. H., "Leaching of chalcopyrite in cupric chloride solution", ***Hydrometallurgy***, 77 (1): 89–95 (2005).

48. Radmehr, V., Koleini, S. M. J., Khalesi, M. R., and Tavakoli Mohammadi, M. R., "Ammonia Leaching: A New Approach of Copper Industry in Hydrometallurgical Processes", ***Journal Of The Institution Of Engineers (India): Series D***, 94 (2): 95–104 (2013).

49. Woodward, T., "On the operability of the Sherritt-Gordon ammonia leach at the Kwinana nickel refinery", Phd, ***Murdoch University***, (2014).

50. Hackl, R. P., "The leaching and passivation of chalcopyrite in acid sulfate media", ***University of British Columbia***, (1995).

51. Barek, J., "How to Improve the Performance of Electrochemical Sensors via Minimization of Electrode Passivation", ***Chemosensors***, 9 (1): 12 (2021).

52. Wang, J., Xie, L., Han, L., Wang, X., Wang, J., and Zeng, H., "In-situ probing of electrochemical dissolution and surface properties of chalcopyrite with implications for the dissolution kinetics and passivation mechanism", ***Journal Of Colloid And Interface Science***, 584: 103–113 (2021).

53. Sharma, S., "Inhibition locale par des molécules organiques de la corrosion intergranulaire précoce du cuivre et effets sur la passivation des joints de grains", These De Doctorat, ***Université Paris Sciences et Lettres***, (2021).

54. Thangavel, V., "Mathematical models for understanding lithium sulfur batteries phenomena", These De Doctorat, ***Amiens***, (2019).

55. Kellogg, H. H., Rao, Y. K., and Marcuson, S. W., "Pyrometallurgy", ***Annual Review Of Physical Chemistry***, 27 (1): 387–406 (1976).

56. Ebin, B. and Isik, M. I., "Chapter 5 - Pyrometallurgical Processes for the Recovery of Metals from WEEE", WEEE Recycling, ***Elsevier***, 107–137 (2016).

57. Ono, K. and Erhard, A., "Ullmann's Encyclopedia of Industrial Chemistry", (2011).

58. Dutrizac, J. E. and Jambor, J. L., "Jarosites and Their Application in Hydrometallurgy", ***Reviews In Mineralogy And Geochemistry***, 40 (1): 405–452 (2000).

59. Szymanowski, J., "Hydroxyoximes and Copper Hydrometallurgy", ***CRC Press***, 456 (1993).

60. Khitab, A., Ahmad, S., Munir, M. J., Kazmi, S. M. S., Arshad, T., and Khushnood, R. A., "Synthesis and Applications of Nano Titania Particles: A Review", ***REVIEWS ON ADVANCED MATERIALS SCIENCE***, 53 (1): 90–105 (2018).

61. Gupta, M., Tomar, R. S., Kaushik, S., Mishra, R. K., and Sharma, D., "Effective Antimicrobial Activity of Green ZnO Nano Particles of Catharanthus roseus", ***Frontiers In Microbiology***, 9: (2018).

62. Jamkhande, P. G., Ghule, N. W., Bamer, A. H., and Kalaskar, M. G., "Metal nanoparticles synthesis: An overview on methods of preparation, advantages and disadvantages, and applications", ***Journal Of Drug Delivery Science And Technology***, 53: 101174 (2019).

63. "Full Article: Gold Nano Particles Synthesized from Magnolia Officinalis and Anticancer Activity in A549 Lung Cancer Cells", **https://www.tandfonline.com/doi/full/10.1080/21691401.2019.1645152** (2022).

64. Lops, C., Ancona, A., Di Cesare, K., Dumontel, B., Garino, N., Canavese, G., Hérnandez, S., and Cauda, V., "Sonophotocatalytic degradation mechanisms of Rhodamine B dye via radicals generation by micro- and nano-particles of ZnO", ***Applied Catalysis B: Environmental***, 243: 629–640 (2019).

65. Calabro, R. L., Yang, D.-S., and Kim, D. Y., "Liquid-phase laser ablation synthesis of graphene quantum dots from carbon nano-onions: Comparison with chemical oxidation", ***Journal Of Colloid And Interface Science***, 527: 132–140 (2018).

66. Fedlheim, D. L. and Foss, C. A., "Metal Nanoparticles: Synthesis, Characterization, and Applications", ***CRC Press***, 348 (2001).

67. "Vapor-Phase Synthesis of Nanoparticles - ScienceDirect", **https://www.sciencedirect.com/science/article/pii/S1359029403000074** (2022).

68. Flagan, R. C. and Lunden, M. M., "Particle structure control in nanoparticle synthesis from the vapor phase", ***Materials Science And Engineering: A***, 204 (1): 113–124 (1995).

69. Mahan, J. E., "Physical Vapor Deposition of Thin Films", Physical Vapor Deposition of Thin Films, 336 (2000).

70. Helmersson, U., Lattemann, M., Bohlmark, J., Ehiasarian, A. P., and Gudmundsson, J. T., "Ionized physical vapor deposition (IPVD): A review of technology and applications", ***Thin Solid Films***, 513 (1): 1–24 (2006).

71. Rossnagel, S. M., "Thin film deposition with physical vapor deposition and related technologies", ***Journal Of Vacuum Science & Technology A***, 21 (5): S74–S87 (2003).

72. Choi, C. J., Dong, X. L., and Kim, B. K., "Characterization of Fe and Co nanoparticles synthesized by chemical vapor condensation", ***Scripta Materialia***, 44 (8): 2225–2229 (2001).

73. Choi, C. J., Tolochko, O., and Kim, B. K., "Preparation of iron nanoparticles by chemical vapor condensation", ***Materials Letters***, 56 (3): 289–294 (2002).

74. Antonelli, M., De Pascale, G., Ranieri, V. M., Pelaia, P., Tufano, R., Piazza, O., Zangrillo, A., Ferrario, A., De Gaetano, A., Guaglianone, E., and Donelli, G., "Comparison of triple-lumen central venous catheters impregnated with silver nanoparticles (AgTive®) vs conventional catheters in intensive care unit patients", ***Journal Of Hospital Infection***, 82 (2): 101–107 (2012).

75. "Liquid Phase Synthesis of Peptides | Nature", **https://www.nature.com/articles/237512a0** (2022).

76. "Ionic-Liquid-Supported Synthesis: A Novel Liquid-Phase Strategy for Organic Synthesis | Accounts of Chemical Research", **https://pubs.acs.org/doi/abs/10.1021/ar030252f?cookieSet=1** (2022).

77. "Full Article: Recent Advances in the Liquid-Phase Synthesis of Metal Nanostructures with Controlled Shape and Size for Catalysis", **https://www.tandfonline.com/doi/full/10.1080/01614940802480379** (2022).

78. Mantzaris, N. V., "Liquid-phase synthesis of nanoparticles: Particle size distribution dynamics and control", ***Chemical Engineering Science***, 60 (17): 4749–4770 (2005).

79. Chen, C. and Chen, Y.-J., "Liquid-phase synthesis of 2-substituted benzimidazoles, benzoxazoles and benzothiazoles", ***Tetrahedron Letters***, 45 (1): 113–115 (2004).

80. Yang, G. and Park, S.-J., "Conventional and Microwave Hydrothermal Synthesis and Application of Functional Materials: A Review", ***Materials***, 12 (7): 1177 (2019).

81. "Hydrothermal Synthesis - MOREY - 1953 - Journal of the American Ceramic Society - Wiley Online Library", **https://ceramics.onlinelibrary.wiley.com/doi/abs/10.1111/j.1151-2916.1953.tb12883.x** (2022).

82. Zhou, Q., Du, D., Lu, C., He, Q., and Liu, W., "A review of thermal energy storage in compressed air energy storage system", ***Energy***, 188: 115993 (2019).

83. Yang, Y., Bremner, S., Menictas, C., and Kay, M., "Battery energy storage system size determination in renewable energy systems: A review", ***Renewable And Sustainable Energy Reviews***, 91: 109–125 (2018).

84. Polat, S., "Dielectric Properties of BN-ZnO-GNP Doped PU-EG Composites", ***International Journal Of Engineering Research And Development***, 13 (2): 635–644 (2021).

85. Chen, H., Cong, T. N., Yang, W., Tan, C., Li, Y., and Ding, Y., "Progress in electrical energy storage system: A critical review", ***Progress In Natural Science***, 19 (3): 291–312 (2009).

86. Chiang, S. J., Chang, K. T., and Yen, C. Y., "Residential photovoltaic energy storage system", ***IEEE Transactions On Industrial Electronics***, 45 (3): 385–394 (1998).

87. Vieira, F. M., Moura, P. S., and de Almeida, A. T., "Energy storage system for self-consumption of photovoltaic energy in residential zero energy buildings", ***Renewable Energy***, 103: 308–320 (2017).

88. Wang, S., Zhang, X., Yang, L., Zhou, Y., and Wang, J., "Experimental study of compressed air energy storage system with thermal energy storage", ***Energy***, 103: 182–191 (2016).

89. Qu, D., "Studies of the activated carbons used in double-layer supercapacitors", ***Journal Of Power Sources***, 109 (2): 403–411 (2002).

90. "Energies | Free Full-Text | A Comprehensive Review on Supercapacitor Applications and Developments | HTML", **https://www.mdpi.com/1996-1073/15/3/674/htm** (2022).

91. Shao, Y., El-Kady, M. F., Sun, J., Li, Y., Zhang, Q., Zhu, M., Wang, H., Dunn, B., and Kaner, R. B., "Design and Mechanisms of Asymmetric Supercapacitors", ***Chemical Reviews***, 118 (18): 9233–9280 (2018).

92. "Supercapacitors Performance Evaluation - Zhang - 2015 - Advanced Energy Materials - Wiley Online Library", **https://onlinelibrary.wiley.com/doi/full/10.1002/aenm.201401401** (2022).

93. "Review on Supercapacitors: Technologies and Materials - ScienceDirect", **https://www.sciencedirect.com/science/article/pii/S1364032115016329** (2022).

94. "Printed Supercapacitors: Materials, Printing and Applications - Chemical Society Reviews (RSC Publishing)", **https://pubs.rsc.org/en/content/articlelanding/2019/cs/c7cs00819h/unauth** (2022).

95. Mashrah, M. and Polat, S., "Hydrothermal synthesis and electrochemical performance of GNPs-doped MgFe2O4 electrodes for supercapacitors", ***Solid State Ionics***, 391: 116107 (2023).

96. "Rational Design of Nanostructured Electrode Materials toward Multifunctional Supercapacitors - Yan - 2020 - Advanced Functional Materials - Wiley Online Library", **https://onlinelibrary.wiley.com/doi/full/10.1002/adfm.201902564** (2022).

97. Polat, S., "Production of ZnFe2O4 Doped Carbon Cloth-Based Flexible Composite Electrodes for Supercapacitors", ***Türk Doğa Ve Fen Dergisi***, 10 (2): 199–205 (2021).

98. Carneiro, M. F. C. and Leão, V. A., "The role of sodium chloride on surface properties of chalcopyrite leached with ferric sulphate", ***Hydrometallurgy***, 87 (3): 73–82 (2007).

99. Liddicoat, J. and Dreisinger, D., "Chloride leaching of chalcopyrite", ***Hydrometallurgy***, 89 (3): 323–331 (2007).

100. Bevilaqua, D., Lahti, H., Suegama, P. H., Garcia, O., Benedetti, A. V., Puhakka, J. A., and Tuovinen, O. H., "Effect of Na-chloride on the bioleaching of a chalcopyrite concentrate in shake flasks and stirred tank bioreactors", ***Hydrometallurgy***, 138: 1–13 (2013).

101. Torres, C. M., Ghorbani, Y., Hernández, P. C., Justel, F. J., Aravena, M. I., and Herreros, O. O., "Cupric and Chloride Ions: Leaching of Chalcopyrite Concentrate with Low Chloride Concentration Media", ***Minerals***, 9 (10): 639 (2019).

102. Zhang, R., Mao, Y., Liu, C., and Ni, W., "Synergistic catalytic effect of chloride ion and ammonium ion on the leaching of chalcopyrite in sulfuric acid solution", ***Minerals Engineering***, 185: 107686 (2022).

103. Petrović, S. J., Bogdanović, G. D., and Antonijević, M. M., "Leaching of chalcopyrite with hydrogen peroxide in hydrochloric acid solution", ***Transactions Of Nonferrous Metals Society Of China***, 28 (7): 1444–1455 (2018).

104. Lu, J. and Dreisinger, D., "Copper leaching from chalcopyrite concentrate in Cu(II)/Fe(III) chloride system", ***Minerals Engineering***, 45: 185–190 (2013).

105. Solís-Marcíal, O. J. and Lapidus, G. T., "Chalcopyrite leaching in alcoholic acid media", ***Hydrometallurgy***, 147–148: 54–58 (2014).

106. Pan, H., Yang, H., Tong, L., Zhong, C., and Zhao, Y., "Control method of chalcopyrite passivation in bioleaching", ***Transactions Of Nonferrous Metals Society Of China***, 22 (9): 2255–2260 (2012).

107. "Synthesis and Electrochemical Performance of MgFe2O4 with G-C3N4 on Ni-Foam as Composite Anode Material in Supercapacitors | SpringerLink", **https://link.springer.com/article/10.1007/s10854-022-09104-w** (2022).

108. Mashrah, M. and Polat, S., "Hydrothermal synthesis and electrochemical performance of GNPs-doped MgFe2O4 electrodes for supercapacitors", ***Solid State Ionics***, 391: 116107 (2023).

109. Polat, S., "Fabrication of CuFe2O4@g-C3N4@GNPs nanocomposites as anode material for supercapacitor applications", ***Ceramics International***, 10 (2022).

110. Majuste, D., Ciminelli, V. S. T., Eng, P. J., and Osseo-Asare, K., "Applications of in situ synchrotron XRD in hydrometallurgy: Literature review and investigation of chalcopyrite dissolution", ***Hydrometallurgy***, 131–132: 54–66 (2013).

111. Munnik, P., Wolters, M., Gabrielsson, A., Pollington, S. D., Headdock, G., Bitter, J. H., de Jongh, P. E., and de Jong, K. P., "Copper Nitrate Redispersion To Arrive at Highly Active Silica-Supported Copper Catalysts", ***The Journal Of Physical Chemistry C***, 115 (30): 14698–14706 (2011).

112. Žic, M., Ristić, M., and Musić, S., "Monitoring the hydrothermal precipitation of α-Fe2O3 from concentrated Fe(NO3)3 solutions partially neutralized with NaOH", ***Journal Of Molecular Structure***, 993 (1): 115–119 (2011).

113. Madhurambal, G. and Mariappan, M., "Growth and characterization of urea-thiourea non-linear optical organic mixed crystal", (2010).

114. Sithole, R. K., Machogo, L. F. E., Airo, M. A., Gqoba, S. S., Moloto, M. J., Shumbula, P., Wyk, J. V., and Moloto, N., "Synthesis and characterization of Cu3N nanoparticles using pyrrole-2-carbaldpropyliminato Cu(II) complex and Cu(NO3)2 as single-source precursors: the search for an ideal precursor", ***New Journal Of Chemistry***, 42 (4): 3042–3049 (2018).

115. Mohamed El Mamy, M., "COPPER FERRITE SYNTHESIS FROM CHALCOPYRITE AND INVESTIGATION OF ITS ELECTROCHEMICAL PROPERTIES", Thesis, (2022).

RESUME

El Moctar MBEBOU completed his primary, secondary and undergraduate education in Mauritania. he graduated from Petit Centre High School in Nouakchott in 2015 and started his education at UNIVERSITY OF NOUAKCHOTT ALASRIYA in the department of geology and graduated in 2019. In 2021 he started his education as a graduate student at Karabuk university (INSTITUTE OF APPLIED SCIENCE) Department of Metallurgy and material engineering